Is Cu Involved in Prion Oligopeptide Stability? Experiments and Numerical Simulations

V. MINICOZZI,[1] S. MORANTE[1,2]

[1]*Dipartimento di Fisica, Università di Roma "Tor Vergata" INFN, Sezione di Roma "Tor Vergata" Via della Ricerca Scientifica, 00133 Roma, Italy*

[2]*CRS—SOFT c/o Dipartimento di Fisica—Università di Roma "La Sapienza" P.le A. Moro, 00185 Roma, Italy*

Received 10 December 2008; accepted 10 February 2009
Published online 23 June 2009 in Wiley InterScience (www.interscience.wiley.com).
DOI 10.1002/qua.22184

ABSTRACT: The high-sociological impact of neurodegenerative diseases (like Alzheimer disease, Transmissible Spongiform Encephalopathies, Parkinson disease, etc.) has renewed the interest of researchers in the study of misfolding processes and in particular of the rôle played by metals in plaque formation as their unbalanced concentration can be regarded as a possible concurrent cause of protein aggregation. Metals are essential players in many of the fundamental activities of cells. Storing, metabolism, and trafficking of metals through the cellular membrane and within the cytoplasm are mediated by many proteins via well-tuned mechanisms because of the toxicity of free ions. In this review article, we summarize the results of the most recent experimental and numerical investigations aimed at understanding the possible rôle of Cu in stabilizing the Prion protein structure and in the formation of protein polymers.
 Int J Quantum Chem 110: 656–680, 2010

Key words: prion; copper; XAS; Car-Parrinello molecular dynamics; density functional theory

1. Introduction

The term Prion, invented by Prusiner in 1982, stands for "proteinaceous infectious protein."[1–3] The Prion is a membrane protein anchored to the cell surface via a glicosyl-phosphatidyl inositol group. It exists in two alternative conformers: the cellular native conformer, PrP^{C}, rich in α-helix (sometimes also called α-PrP), and the pathogenic conformer, PrP^{Sc} (or scrapie PrP) endowed with aberrant self-replicating properties, with a comparatively higher β-sheet content (hence sometimes also called β-PrP) [4].

The PrP^{Sc} conformer displays dramatically different biochemical properties with respect to ordi-

Correspondence to: S. Morante; e-mail: morante@roma2.infn.it
Contract grant sponsor: PRIN05.
Contract grant number: 2005023002.

nary PrP^C, despite having the same chemical composition. Possibly because of its high β-sheet content, PrP^{Sc} is, in fact, prone to form protease-resistant amyloids that accumulate in several tissues of the organism (mainly in brain, but also in the lymphatic system).

Prion diseases are characterized by the over-stabilization of the alternative conformers, PrP^{Sc} [5]. Accumulation of PrP^{Sc} appears to be strictly related to the insurgence of fatal neurological diseases belonging to the class of Transmissible Spongiform Encephalopaties (TSE's), such as the Creutzfeldt–Jakob disease in humans (in its various forms, sporadic, familial, iatrogenic, and variants), scrapie in sheep (after which the pathological conformer is named), Bovine Spongiform Encephalopathy in cattle, etc. (see Ref. [3] for a review).

TSE's in their many variants belong to a larger family of neurodegenerative diseases, generically called *amyloidosis* which are all caused by the transition of endogenous proteins (or peptides) from the physiological globular configuration to a pathological fibrillar state. Amyloidosis comprise a heterogeneous group of diseases (more than 20), characterized by the extracellular deposition of fibrillar proteic material [6] among which we find Alzheimer and Parkinson diseases to mention two of the most devastating pathologies affecting a large fraction of the elder people in the world. Independently of the nature of the amyloid protein by which they are formed, fibrils have a common ultrastructure. They grow, unbranched, to a variable length that may reach several microns, with a diameter of 7–10 nm. They are organized in a characteristic helicoidal β-structure and are able to bind to Congo Red dye generating a typical birefringence, a phenomenon which is commonly used as a test to detect their presence.

Although the social impact of Alzheimer or Parkinson disease is certainly not comparable with that of TSE, we will limit ourselves in this review to the study of the Prion protein because the latter represents the prototype of a protein capable of aberrant foldings with self-replicating properties. For this reason, PrP has been, indeed, the object of a large number of experimental and theoretical investigations, which laid the ground for the extension of ideas and methodologies first developed there to the case of other, perhaps more dramatically relevant, neurodegenerative amyloid pathologies.

1.1. THE PRION PROTEIN

The Prion protein is made out of about 260 amino acidic residues, with this number slightly varying from species to species. The C-terminal domain of PrP^C is structured and its structure has been solved by both Nuclear Magnetic Resonance (NMR) and X-ray diffraction techniques (see for instance Ref. [7] and references therein). The N-terminal region is instead unstructured and characterized by a highly conserved domain made of a variable number (from four to six depending on the species) of the tandemly repeated sequence of the eight amino acidic residues, PHGGGWGQ, termed *octarepeat* in the following. The lack of structure of the octarepeat region is attributed to the presence of a rather large number of the very-flexible glycine (Gly) residues. Even though the structural changes leading to the conversion of PrP^C into PrP^{Sc} occur at the C-terminal domain, the N-terminal octarepeat region seems to play a regulatory rôle in the overall process [8–11].

Among the different biochemical functions tentatively attributed to PrP^C, copper ion (Cu^{2+}) binding is, to date, the only one that has been correlated with the physiological impairments linked to the disease [12–15]. PrP—Cu^{2+} binding was first described in the protocol tailored for PrP^C purification. The histidine (His) residues located within the octarepeat region have been identified as metal ligands [16–20]. Studies with PrP^C models in the form of synthetic and recombinant peptides have shown binding stoichiometries of up to one Cu^{2+} per octarepeat motive. Furthermore, positive cooperativity among cation sites is seen to occur when the number of saturated binding sites is larger than two [21–23]. In addition to the octarepeat region, other Cu^{2+} binding sites in the C-terminal globular domain have been reported [24–26].

From all these results, it clearly emerges that the key point that needs to be clarified is how the interaction with Cu^{2+} affects the biochemistry of PrP.

Interestingly, recent experimental results (coming from X-ray Absorption Spectroscopy—XAS [27] and Electron Paramagnetic Resonance (EPR)[28] data) have provided structural evidence that at low-Cu occupancy, two or even more, His's can be coordinated to the metal. Any confirmation of this finding is clearly of the utmost importance. In fact, since each octarepeat contains only a single His residue, a two-His coordination mode would mean that Cu is able to bind two octarepeats belonging

either to the same PrP molecule or to two distinct molecules. This fact hints at a significant rôle of Cu in at least the first steps of the protein aggregation process. The subsequent steps of mesoscopic fibril formation may on the contrary have a protective effect against neurodegenerative processes [29–31]

An important physico-chemical parameter in this context is the level of protonation vs. deprotonation state of amide ligands. Indeed, as illustrated in the seminal paper of Ref. [32] in Cu-peptide complexes, the metal can promote peptide hydrogen deprotonation, thus somehow mimicking a local pH change. This is in agreement with the results of [19] which show that, in the peculiar five-membered chelate ring structure which Cu takes when it is coordinated to the HGGG peptide, the metal ion is capable of replacing the amide proton of Gly at neutral pH.

The occurrence of this deprotonation phenomenon in at least one of the two Gly nitrogens involved in Cu binding has been confirmed in recent first principle simulations of the Car-Parrinello (CP) type [33], giving evidence for the existence of a thermally accessible mechanism for amide deprotonation at neutral pH. More generally in that work the coordination geometry of Cu to the HGGG peptide was studied in detail, finding results in nice agreement with the experimental data of Ref. [19]. In particular it was found that Cu is bonded to the amide nitrogen of the two adjacent deprotonated Gly residues lying next to the His residue, and to the nitrogen of the imidazole ring of the latter. In addition, evidence was given that nitrogens from deprotonated Gly's are more strongly bonded than the $N_{\delta 1}$ of the His imidazole ring. Although it was observed that Cu^{2+} stabilizes the formation of the $[Cu^{2+}\text{-HGGG}]_2$ [33], the key question which one still needs to answer in this context is whether a second His can be bound to Cu and to what extent this binding depends on the deprotonation state of the amide nitrogens of the two adjacent Gly's lying next to the His residue.

To try to clarify these points, extensive CP Molecular Dynamics (CP-MD) simulations of solvated Cu^{2+}-HGGG complexes with the bonded Gly residues in various amide deprotonation states and in interaction with a second His have been recently carried out [34].

These numerical simulations have been complemented by configuration stability analysis, where selected snapshots of the simulated systems, taken from the collected CP-MD trajectories and representative of the different chemical complexes of interest, have been subjected to geometrical optimization so as to compare the formation energies of related dissociated subsystems. In this way, the degree of stability of the various involved chemical species could be determined.

The main result of this rather detailed analysis is that the presence of a second His (viz. of a second octarepeat) bound to Cu stabilizes the complex independently of the protonation state of the other bonded Gly's.

1.2. OUTLINE OF THE REVIEW

The content of this review is as follows. We start in section 2 with a general introduction on the experimental techniques, in particular XAS, that have been employed to investigate the structure of the metal binding site in metal-protein complexes, and the parallel use of ab initio simulations aimed at understanding the molecular basis for the atomic geometrical arrangement of the metallic site. In section 3, we describe in some detail the experimental information that has been collected in the years about the Cu coordination mode in Cu—PrP complexes. The ab initio simulations that have been recently carried out on model systems of Cu—PrP are illustrated in section 4, where we also describe the nature of the configurational stability studies that have been carried out on a number of Cu—PrP complexes and the interesting results that have been obtained. Conclusions and an outlook on future lines of investigations can be found in section 5.

2. Experimental and Theoretical Methods

Many experimental techniques have been used with the purpose of characterizing the structure of the metal binding site in amyloid complexes, among which crystallography [19], EPR [28, 35, 36], NMR [37–39], Circular Dichroism (CD)[35, 36, 39], and XAS [27, 40–42] are the most prominent ones.

In particular, the availability of third generation synchrotron radiation sources has greatly enlarged the range of applications of XAS in the investigation of structural properties of biological systems. Reliable data for a wide range of absorbing atoms, even if often very diluted as it is typical in this field, are now accessible. XAS can be, in fact, successfully used to study the environment of metal ions com-

plexed with proteins and peptides in physiological conditions, owing to its chemical selectivity and sensitivity to the local atomic neighborhood around the absorber. An accurate analysis of the extended X-ray Absorption Fine Structure (EXAFS) region of the spectrum in terms of single plus multiple scattering (MS) events allows a clear-cut identification of the amino acid residues primarily bound to the metal. A well-known example of application of this technique is to metal-enzymes, where the metal plays either the rôle of maintaining the protein active conformation or of acting as a catalytic center [42–45].

As for the theoretical interpretation of the wealth of today available experimental data, routine techniques used to model atomic interactions (like Monte Carlo and Molecular Dynamics (MD) simulations on the one hand and Quantum Chemistry (QC) and Density Functional Theory (DFT) calculations on the other), though still limited by the insufficient accuracy of present computational methods, are steadily increasing their capability of investigating the supramolecular level. Indeed, advances in algorithm development, software implementation, and hardware upgrading are rapidly improving the situation in a very promising way.

As we already said, understanding the peculiar electronic properties of metal complexes is a necessary step to clarify the rôle played by metal ions in biochemical reactions. This means that the electronic structure of the compound need to be described at the quantum level, i.e., in the framework of DFT and will require special techniques for application to biomolecules. For instance, the use of the standard plane-wave expansion for expressing the electron density in quanto-mechanical calculations is often considered particularly well-suited for dealing with delocalized systems like organo-metallic molecules, especially when coupled with the use of ultrasoft pseudo-potentials for the description of the electronic atom core [46]. The plane-wave approach is to be preferred in this context because it allows the use of a coarse grid for the representation of the delocalized electron density together with a finer grid for the localized electron density around the atomic nuclei. In this way, the number of necessary plane waves is drastically reduced and ab initio molecular dynamics simulations, for instance, of the CP type become feasible [47].

2.1. X-RAY ABSORPTION SPECTROSCOPY

From the experimental point of view, this review will be focused on the XAS technique, as the latter displays a number of very interesting features when it is employed in investigating biological systems, and especially in the study of metal-proteins [27, 42, 43, 44, 48]. Perhaps, the most important of them is that XAS can be used for samples in any state of aggregation. A further advantage with respect to other spectroscopic techniques is that there are no selection rules that would extinct the signal in unlucky circumstances, with the result that a XAS signal is always present. Finally, XAS is very sensitive to the nature of the metal absorber. It allows extracting structural information about the absorber atomic environment through the study of the oscillations of the absorption coefficient originating from the interference between the outgoing electron wave, kicked-off from the metal, and the back-scattered waves emerging from the atoms surrounding the latter [49–52]. The interference spectrum contains detailed information about scatterer-absorber relative positions, from which the geometrical and structural arrangement of the amino acids that are coordinated to the metal can be inferred with fairly good accuracy. Data analysis requires a rather sophisticated theory, though, where single and multiple scattering contributions [53, 54] must be taken into account.

2.1.1. Generalities

XAS uses Synchrotron Radiation as source of photons. We recall that for any absorption process the following very general law holds:

$$I(E) = I_0(E)e^{-\mu(E)d}, \tag{1}$$

where $E = h\nu$ is the energy of the incident photon, $I(E)$ is the intensity of the transmitted radiation, $I_0(E)$ is the intensity of the incident radiation, $\mu(E)$ is the absorption coefficient characteristic of the system in consideration, and d is the thickness of the sample traversed by the photons.

The behavior of the absorption coefficient, $\mu(E)$, with the photon energy is monotonically decreasing except where the photon energy corresponds to the photo-ionization energy, E_0, of an inner electron of the absorbing atom. Around this energy, the absorption coefficient rapidly increases and, if the absorbing atom is isolated (for example when a

monoatomic gas is considered), it starts to decrease soon after the edge energy.

The photo-ionization energy of an inner electron is usually referred to as the "edge energy" or simply the "edge." The *K*-edge corresponds to the ionization of one of the innermost electrons, whereas the *L*-edges correspond to the ionization of the electrons belonging to the next electronic shell, and so on.

At a sufficiently high-atomic number, the edge energies of the various atoms are well-separated, so that the absorbing spectrum of a complex system shows characteristic peaks. These peaks, which are in correspondence with the edge energies of the various atomic species, are well-distinguishable from one another. Just to give an idea, the *K*-edges of Fe, Cu, and Zn are located at 7112, 8979, and 9659 eV, respectively. This is the reason which makes XAS such a highly selective technique and allows to get detailed local structural information around a selected atom.

In a multiatomic system, the value of the absorption coefficient does not decrease monotonically after the edge, as it does for an isolated atom, but it has an oscillating behavior. The physical explanation for the oscillating behavior of $\mu(E)$ has its roots in the quantum interference phenomenon. To a very-good approximation, the wave function of the ionized electron (photo-electron in the following) can be described as an outgoing spherical wave centered on the absorber. The atoms surrounding it act as diffusion centers (scatterers) for the impinging wave. In turn, the back-scattered waves from the atoms around the absorber interfere with the outgoing spherical wave of the photo-electron. The interference will result in a modulation of the wave function of the photo-electron. As a result, the probability for the photon to be absorbed shows maxima or minima, according to whether the outgoing and scattered waves are *in phase* or *out of phase,* respectively. Amplitudes and phases of undulations will depend on the kind and relative position of absorber and scatterers or, in other words, on the chemical and structural (three-dimensional) arrangement of the absorber atomic environment. This is the same as saying that the interference signal contains information about the local geometrical structure around the absorber.

2.1.2. The XAS Spectrum

The XAS spectrum is commonly separated into two energy regions:

1. The XANES, X-ray Absorption Near Edge Structure, region that starts few eV before the edge energy, E_0, and extends a few eV above it;
2. The EXAFS region that follows the XANES region and extends some few hundreds eV above the edge.

The XANES region is dominated by MS processes, where the photo-electron undergoes more than one scattering event either with different scatterers or more than once with the same scatterer. In principle, it contains many detailed information about the local atomic structure around the absorber. Unfortunately, these potentialities could not yet be fully exploited, because of the difficulty of setting up a reliable theoretical analysis of this energy region. There is, in fact, quite a number of reasons why it is problematic to describe this part of the spectrum or extend to it the procedure used in discussing the EXAFS region (see below). Among them, we may mention the inadequacy of the muffin-tin approximation [55] to the interatomic potential at-low photo-electron energies, the lack of a satisfactory description of screening, and relaxation processes following the sudden creation of a core hole, the need of including electronic correlations and, in particular, two-electron excitations, etc.

Because of the difficulties in modeling in an adequate way these complicated processes, the analysis of XANES region has remained for a long time at a semi-qualitative level. Only, very recently methods have been proposed [56] capable of yielding a semi-quantitative analysis of the region from the edge up to about 200 eV above threshold, which was used in a number of interesting situations [57]. Its wider application is still limited to cases, where a quite precise idea about the geometrical arrangement around the absorber is available.

The kinetic energy, E_k, of the photo-electron, which is given by the obvious formula as follows:

$$E_k = h\nu - E_0, \tag{2}$$

is larger in the EXAFS region compared with the values it takes in the XANES region. At higher-electron energies, single scattering events are dominant. However, MS contributions, that are richer in structural information, are still present and must be taken into account in analyzing experimental data [51, 53, 58].

Theoretical approaches [53, 59] giving a rigorous quantum-mechanical description of the EXAFS signal, including both single and multiple scattering terms, have been implemented in a number of packages among which we may mention gnXAS [60], FEFF [61], and Excurve [62, 63]. For a review see Ref. [55].

The inclusion of MS terms in the analysis of XAS data is especially important in investigating the structure of the active site in a metal-protein. Amino acidic residues are, in fact, almost completely made of "light" atoms (i.e., nitrogen, oxygen, and carbon) and their contributions to the total XAS signal are indistinguishable from one another, if the analysis is performed in the single scattering approximation. Including MS contributions removes to a large extent this limitation. The magnitude of the contributions coming from the presence of amino acids around the metal absorber, in fact, turns out to depend not only on the kind and mean distance of the atomic scatterers, but also on the specific geometrical arrangement they take. A well-known and biologically very important example of this situation is represented by the case of histidine. The presence of this residue bound to a metal can be easily identified in a XAS spectrum because the contribution it gives to the signal through MS events is strongly enhanced owing to the positive interference of amplitudes (focusing effect) resulting from the collinearity of the atoms belonging to the His imidazole ring with the absorbing atom [64]. A remarkable example of this situation is the interplay between the structure of the active site in a metal-protein and its functionality enlightened in the work of Ref. [45].

2.2. AB INITIO SIMULATIONS

As a fundamental tool for the interpretation of experimental results, in this review, we want to show how ab initio simulations (in particular of the CP type) can be profitably used to understand structural data and discriminate among different models thanks to the detailed atomic information that numerical methods can provide.

CP-MD simulations have been largely and very successfully used in many research areas ranging from solid state physics to biological systems. Among the numerous papers in these areas, see for instance those quoted in Refs. [65, 66], respectively. In applications to metal-protein complexes, CP-MD was employed and validated in the detailed structural study of the Cu binding sites located in the unstructured octarepeat region of the Prion protein carried out in Refs. [33, 34, 67].

The use of quantum mechanical (QM) methods (as opposed to purely classical MD approaches) for computing the force field felt by atoms is mandatory in the study of metal-protein complexes for two reasons. One is of a technical nature and has to do with the presence of a metallic (doubly charged) ion in the system, which makes much safer the use of first principle simulations, for they embody charge polarization and screening, rather than that of classical MD which would require employing one of the rather sophisticated, but still not fully satisfactory, algorithmic tricks that have been developed to deal with the situation where the long range Coulomb interactions are present [68]. The second reason is more fundamental and it is related to the fact that it is the main purpose of all structural studies to identify the nature of metal ligands. This is of course something which is not known a priori and should be the main outcome of the investigation rather than an input as would be the case if one decides to employ classical atomic force fields.

An obvious limitation to the use of quantum mechanical numerical simulations is the foreseeable very-short length of the CP-MD trajectories (few picoseconds) for systems of the size one is interested in biology that can never be as extended as one would like them to be. We certainly do not intend to evaluate anything like *ensemble* averages along such short trajectories. The interest of using CP-MD simulations is rather that unstable configurations are easily spotted along the system time history; even if the latter is rather short, as atoms immediately tend to move away from their initial positions if the system is not near to any stable or long-living state.

An alternative possible way to cope, at least partially, with the difficulties related to the conflict between the need to deal with a realistically large system and the consequent limitation concerning the length of the simulated trajectory could be to exploit the possibilities offered by the recently developed mixed classical/quantum mechanical methods, like QM/MM [69]. We should say that in the present situation, these methods are quite well-suited as it is immediately obvious which part of the system should be treated quantum-mechanically (the metal ion and the "nearest atoms" surrounding it) and which other part can be treated classically (the "rest" of the peptide and the solvent).

Apart from this possibility, there are good reasons (supported by quite a long experience in the field of CP-MD simulations) which make one to believe that already a few picoseconds trajectory can give useful information on structural problems like those we are interested in this project (i.e., identification of primary metal ligands). The argument is based on the observation that CP-MD simulations can be thought as a way of successively computing the electronic density while atoms move gently around in a quantum mechanical potential which is generated on the fly. From this perspective, CP-MD may be considered not so terribly different from genuine DFT or QC computations [70-72], provided one can live with the two well-known problems of the CP-MD method. Namely, the fact that excited electronic states are essentially inaccessible (see however [73]) and that atoms will only be able to explore a region of the phase space not too distant from their initial configuration.

It is very important to stress that the application of CP-MD methods to the study of metal-proteins is not set back by any of these two limitations. In fact, what one would like to identify and characterize are the different coordination modes of Cu when complexed with the various fragments of the Prion protein considered in experiments. Indeed, the focus in this framework is in understanding what could be the specific rôle of the metal just in the very first steps of a possible aggregation process, where equilibrium is not yet an issue. This more modest approach is still of great relevance because it looks that only the aggregates that are formed in the very early stage of this biochemical pathway are pathological. The subsequent steps of mesoscopic fibril formation may on the contrary produce compounds that have a protective effect against neurodegenerative processes [29, 30, 31]. In any case, fibril formation is driven by an extremely complicated dynamics, which at the moment is beyond any possible quantum mechanical description.

As for the problems related to an insufficient phase space exploration, they are in general of the greatest importance in numerical simulations, but in the case we are discussing in this review they are well kept under control because the system configurations from which CP-MD simulations are started from are taken either from experimental structural data (XAS, NMR, EPR) or from longly equilibrated classical trajectories. Furthermore, one is in the rather favorable situation where the very compact arrangement detected in experiments (see, for instance, the crystallographic structure of PrP around a coordinated Cu ion shown in Fig. 1), that the peptide takes in the presence of the metal, significantly reduces the magnitude of the actually accessible phase space.

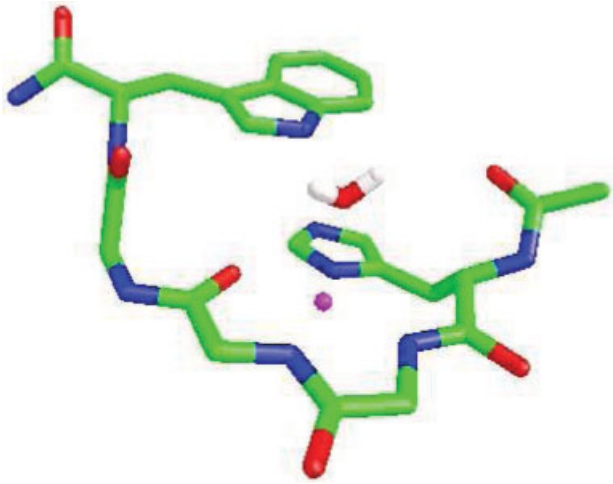

FIGURE 1. The crystallographic structure of the HGGGW penta-peptide belonging to the octarepeat region of the Prion protein [19]. Colors are as follows: white is H, red is O, green is C, blue is N, and magenta is Cu. [Color figure can be viewed in the online issue, which is available at www.interscience.wiley.com.]

3. Experimental Structural Studies of Cu–PrP Complexes

In this section, we will present and discuss a selection of the many experimental results that have been collected in the study of the Cu coordination mode in complexes with the Prion protein and a summary of the phenomenological interpretation of these data.

3.1. CU BINDING SITES

From the many experiments carried out in the recent years, different models for the structure of the Cu^{2+} binding sites located along the PrP amino acidic sequence have been proposed to date. In particular, two kinds of models have been proposed for the geometry of the Cu binding site in the octarepeat region of PrP.

In one group of models, based on CD, EPR, and NMR experiments, Cu^{2+} has been proposed to be coordinated to two His residues, thereby bringing into close contact successive octarepeats [12, 21].

TABLE I

Cu^{2+}-complexes of BoPrP-(24–242) and its templates synthetic peptides subjected to XAS measurements.

P1	BoPrP-(25–30,60–70)	KKRPKPWGQPHGGGWGQ
P2	BoPrP-(25–30,60–78)	$KKRPKPWGQ(PHGGGWGQ)_2$
P3	BoPrP-(25–30,60–94)	$KKRPKPWGQ(PHGGGWGQ)_4$
P4	αBoPrP (24–242)	BoPrP-(24–242)

The initial KKRPKPWGQ sequence in samples P1, P2, P3 has been added to increase peptide solubility.

These models were elaborated on the basis of results obtained in experiments with a substoichiometric complexation of Cu^{2+} per octarepeat.

The models of the second group are based on the crystallographic structure of Cu^{2+} in complex with the minimal HGGGW binding site [19] and have been considered to be relevant for the fully saturated α-PrP-(23–231) protein [19, 26, 37]. In these fully saturated forms, Cu^{2+} is penta-coordinated with the nearly equatorial ligation to the δ_1 nitrogen of the His, the deprotonated amide nitrogens of the two sequential Gly residues, the amide carbonyl oxygen of the second of these two Gly residues, and the axial ligation of the oxygen of a water molecule hydrogen bonded to the triptophane (Trp) indole ring (Fig. 1).

As for the binding sites other than those involving the octarepeat region, XAS experiments on human PrP-(90–231) in complex with Cu^{2+} have clarified the geometry of the site involving the sidechains of His_{96}, Gln_{98}, Met_{109}, and His_{111} [24]. In N-terminal domain truncated PrP forms [14, 24], this site appears to be endowed with a particularly high-affinity for Cu.

3.2. CU COOPERATIVITY

It has been argued in Ref. [18] that the Cu coordination mode in the two regions of the Prion protein encompassing residues 57–91 (which contains the four octarepeats) and residues 91–115 depends on the number of bound Cu ions. This finding seems to suggest a precise rôle for Cu^{2+} in controlling in vivo PrP self-association and rises the question of cooperativity in Cu^{2+} binding.

Similarly titration experiments monitored by CD and fluorescence spectroscopy have reported that Cu^{2+} binding to PrP shows positive cooperativity with a Hill coefficient of ≈ 3 [21–23]. A possible interpretation of cooperativity of Cu^{2+} binding is in terms of a transition from an intramolecular interrepeat geometry to an intrarepeat structure. This transition is quite significant as it involves the passage from a long range to a short range structure. It appears to be not only a function of the Cu^{2+} saturation degree but also to depend on the number of octarepeat copies. In fact, many studies [21–23] have confirmed that cooperativity of Cu^{2+} binding shows up for PrP forms containing more than two octarepeat copies. The XAS analysis [27] agrees with this observation (see below), further suggesting that the binding of copper by the His's of two successive octarepeats is disfavored, and that the two stapling His's should be at a minimum repetition distance of three octarepeats (at variance with the models proposed in Refs. [12, 21]).

3.3. XAS EXPERIMENTS ON PRION PROTEIN

XAS has been extensively employed in the study of the recombinant bovine PrP,[1] folded into a PrP^C-like conformation (αBoPrP-(24–242)), in complex with Cu^{2+}. To better clarify the structure of the binding site, besides αBoPrP, also Cu^{2+} complexes of synthetic peptides containing either one, two, or four octarepeat copies have been subjected to XAS measurements. The whole set of Cu^{2+} complexes that have been analyzed together with their amino acidic composition are displayed in Table I. XAS spectra at various Cu concentration levels have also been taken.

A detailed analysis of all the collected EXAFS data was performed in Ref. [27]. The study has revealed the existence of two kinds of Cu binding geometries differing in the number of coordinated His imidazole rings. In one structural arrangement, Cu is coordinated like in the crystallographic structure of the minimal site [19] (Fig. 1), with only one single imidazole ring within the metal coordination sphere (see panel A of Fig. 2). This geometry is realized when Cu^{2+} is in complex with synthetic

[1]Bovine PrP contains five octarepeats, or rather four identical octarepeats plus a fifth slightly different one.

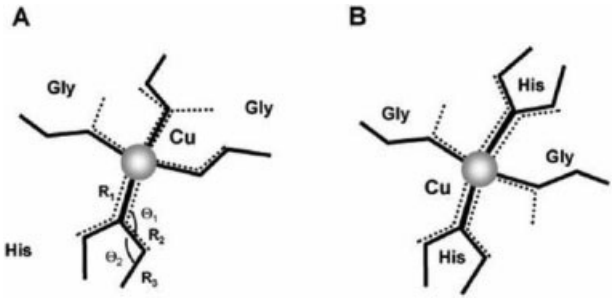

FIGURE 2. Cu coordination mode from EXAFS data best fit. Panel (A) shows intrarepeat Cu geometry resulting from a single imidazole ring binding. Panel (B) shows inter-repeat Cu geometry resulting from a two imidazole rings binding structure.

peptides containing up to two octarepeats (samples P1 and P2 of Table I). The analysis suggests that we are in the presence of a metal mediated intrarepeat binding mode.

The EXAFS data analysis of Cu^{2+} in complex with both the full length αPrP and the four-octarepeat peptide (samples P3 and P4 in Table I) indicates that Cu, at variance with the previous situation, is now coordinated with two equatorial nitrogen atoms from two His imidazole rings (panel B of Fig. 2). Since in each octarepeat only a single His residue is present, it is concluded that the configuration with two bound His residues arises as a result of an inter-repeat (possibly inter-molecular) Cu-mediated binding interaction. It should be observed here that in this structural situation, we do not expect the two metal paired repeats to be two consecutive octarepeats belonging to the same peptide, because of steric effects (Fig. 3).

A further interesting point emerged in studying the result of varying the Cu^{2+} saturation when the metal is complexed with the four-octarepeat peptide P3. Indeed, when the Cu^{2+}-to-octarepeat molar ratio is increased from 0.5 to 0.8, the characteristic features of the XAS spectrum related to the presence of His's display a transition from the shape typical of His multiplicity equal to two to that typical of multiplicity one, thus signaling an inter-repeat to intrarepeat modification of the binding geometry. In the cartoon shown in Figure 3, the peptide aggregation mode as function of Cu concentration is depicted.

In conclusion, the existence of two types of Cu^{2+} sites in the octarepeat region of αPrP correlated with Cu^{2+} saturation level, revealed by XAS, can explain both the participation of the protein in molecular homo- and hetero-assemblies through the N-terminal domain and the basis for the cooperativity of the cation binding process.

4. Ab Initio Simulations

In this part of the review, we want to discuss how ab initio simulations can be profitably used to interpret experimental results and possibly discriminate among different models owing to the detailed atomic information that numerical methods can provide.

In section 4.1, we summarize what has been done within the DFT approach, whereas in the remaining sections (from section 4.2 to 4.6) we present and discuss the large body of results that have been produced using ab initio simulations of the CP type.

In this second part, after a short introductory discussion on some important issues related to the CP-MD simulation strategy and the code, we will

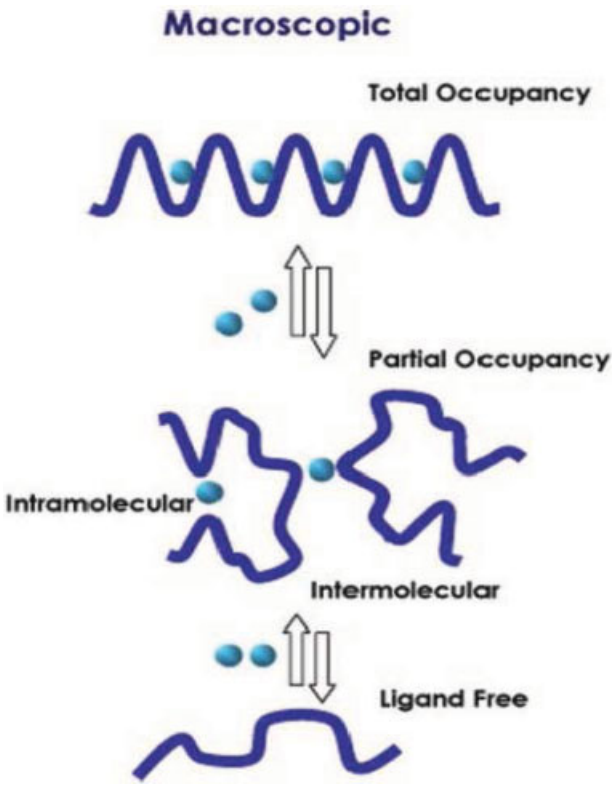

FIGURE 3. Peptide aggregation mode at varying Cu concentration. Cu concentration decreases from top to bottom. [Color figure can be viewed in the online issue, which is available at www.interscience.wiley.com.]

mainly concentrate on in this review (subsections 4.2.1 and 4.2.2), we will discuss two sets of interesting Cu—PrP complex simulations. The first set of simulations was carried out in Ref. [33] with the aim of confirming the claimed Cu binding site crystallographic structure and studying the possibility to form dimeric compounds at high-Cu concentration (subsections from 4.3.1 to 4.3.5). The main purpose of the second, more recent, set of simulations [34] was to extend the previous investigation to low-Cu concentration with the purpose of studying the ability of a single Cu ion to bind more than one His (subsections from 4.4 to 4.5.1) and the influence of pH on the stability of the resulting compound (subsection 4.6).

4.1. OLDER NUMERICAL RESULTS

The coordination mode of the Cu^{2+} ion suggested by the existing experiments and shown in Figure 1, in which the metal is bound to the protein backbone, is somewhat unusual for a metal-protein, though it has been identified in a number of Cu-peptide complexes [32, 74]. In these complexes, the Cu^{2+} ion is seen to be directly bound at pH $\approx$ 7 to the peptide backbone through the deprotonated amide nitrogens of two nearby Gly residues. This finding is rather interesting as it means that a Cu ion is able to replace one or two amide protons of the backbone, possibly affecting conformational transitions in proteins and other molecules in the vicinity.

Despite the large amount of experimental evidence for the Cu—N(Gly) bond stability, only a few theoretical works have confirmed this observation in a quantum mechanical framework. DFT calculations performed on several models of the Cu(HGGG) molecule measured an energy change of roughly -100 kJ/mol upon Cu binding in the stable square-planar (3N1O) coordination [75]. In this coordination, the third nitrogen comes from the imidazole ring of the His of the HGGG motif, whereas O is the carbonyl oxygen of the second Gly. Moreover, in another DFT study [76], the energy of the crystal coordination was found to be slightly higher than that of the coordination, where the carbonyl oxygen is replaced by a water molecule. Both DFT calculations consistently confirmed that in the singly occupied site, the HGGG ligand is able to accommodate the two Cu—N(Gly) stable bonds observed in the crystal [19] and NMR [37] resolved structures. The interplay between ligand flexibility and Cu quantum mechanics makes the study of Cu coordination to the PrP an ideal arena for CP-MD simulations.

4.2. CAR-PARRINELLO AB INITIO SIMULATIONS

We now discuss the general strategy underlying the CP approach and give an account of the many interesting results that have been recently obtained. We also provide a brief description of the code with the help of which all these results were obtained and we will comment on the very important issue of the CPU times necessary for numerical studies of systems of biological interest of the kind we are dealing with here.

4.2.1. The General Strategy for CP Simulations

A key issue in CP-MD simulations is the structure of the atomic configuration, which should be used to start the simulation. Given the effectively rather short time duration of any CP trajectory, it is, in fact, mandatory to start from a very accurately equilibrated and thermalized configuration to avoid biases and instabilities. To cope with this problem, a rather elaborated two-step procedure was devised [33].

First of all, the initial atomic configuration for the successive CP-MD should be obtained at the end of some very-long (few tens of ns) classical MD simulation. For this purpose, preliminary MD simulations using any of the available MD codes (like GROMACS [77], Amber [78], etc.) must be carried out.

Secondly, according to well-tested experience, one has to proceed to minimize stresses and strains among atoms while electrons are pushed to vanishing temperature. To this end, one has to perform CP-MD simulations according to the general protocol, which consists in the four sequential steps listed below:

1. Minimization of electronic energy with fixed atomic positions.
2. Minimization of total energy as a function of both atomic and electronic degrees of freedom of the full system.
3. Two (or more, according to needs) short preliminary sequential CP-MD simulations at increasing atomic temperatures, using a Nosé-Hoover thermostat [79] coupled to the atomic

degrees of freedom, and kept at the desired temperature.

4. The final CP-MD simulation of appropriate length at an atomic temperature of 300 K, using the same thermostat as in 3.

Thermalization in step 3 is necessary to slowly attain room temperature, avoiding that temperature oscillations affect in an uncontrolled way the approach of electrons to their ground state. The velocity-Verlet algorithm [80], for integrating the CP equations of motion, is most commonly used.

The key question at this point is how long the simulated CP-MD trajectories can be. The answer depends obviously on the size of the system (i.e., volume, number of atoms, N_{at}, and number of electrons, N_{el}) and the CPU power of the available machines. A careful analysis of the dynamics underlying CP-MD [81, 82] reveals that an acceptable time step turns out to be extremely small, of the order of 0.10–0.15 fs. Detailed feasibility studies on systems with large number of atoms (from 400 to about 10^3) and electrons (from 10^3 to 2.5×10^3) have been carried out on different machines (PC clusters as well as large parallel platforms), using the two CP available codes, namely Quantum ESPRESSO (QE)[83] and CPMD [84]) in some of their various versions. The result of this thorough investigation is that on a large parallel machine on a 128 nodes configuration and for the largest of the systems tried one needs something like 250–300 h of CPU time for a 1.2 ps trajectory. From this estimate, one can infer that a full-fledged simulation following the protocol illustrated above would require something like a factor of 10 more time per each simulated system. The conclusion that emerges from this analysis is that at the moment it is very hard to go beyond O(10) ps for the kind of systems we are discussing in this review. The situation is not as bad as one might think, however, because, as we shall see, even a few ps trajectory (if the initial configuration has been carefully chosen) contains quite a lot of useful dynamical information about the structural stability properties of the system.

4.2.2. The Quantum ESPRESSO Package for CP-MD Simulations

A parallel version of the freely-available Quantum-ESPRESSO package (opEn-Source Package for Research in Electronic Structure, Simulation, and Optimization [46, 83]) which incorporates Vanderbilt ultrasoft pseudopotentials [85] and the PBE exchange-correlation functional [86] was used for most of the simulations discussed in this review. Electronic wave functions are expanded in plane waves up to an energy cutoff 10 times smaller than that used for the expansion of the augmented charge density in the proximity of the atoms, as required by the ultrasoft pseudopotential scheme. The choice of ultrasoft pseudopotential is dictated by the fact that otherwise the presence of light atoms (like hydrogen, nitrogen, oxygen, and carbon) in biological systems would have required an impossibly high-cutoff when standard norm conserving pseudopotentials are employed.

To minimize finite volume effects, periodic boundary conditions are imposed to the system. This choice has the extra bonus that the resulting geometry is well-suited for plane wave expansion. The molecule is inserted in a box (filled with water molecules at 1 g/cm^3 density) with sufficiently large linear dimensions to ensure a separation between nearest replicas of the system so as to have negligible spurious self-interactions. For neutral systems, a separation of 4–5 Å is considered to be sufficient. For charged systems, a separation of 7–8 Å is required.

CP-MD calculations are often performed ignoring the spin degree of freedom of the electrons, i.e., in the so-called spin-restricted conditions. This approximation is adequate for the kind of systems we are interested in here. In Ref. [33], the realm of applicability of this simplified computational approach in this field was studied with the conclusion that the effect of the spin polarization is negligible and can become relevant only when two or more metal ions are simultaneously present.

4.3. Cu BINDING MODE IN THE PRP OCTAREPEAT REGION

In the next few subsections (from section 4.3.2 to 4.3.5), we describe the numerical evidence that has been collected in ab initio simulations confirming the peculiar nature of the Cu binding mode in the PrP octarepeat region. Then starting from section 4.4, we present a summary of the latest studies on the ability of Cu to bind two His at the time together with the results of a detailed analysis of the stability of this configuration with the deprotonation state of the bound Gly's.

The starting point of all these investigations was the crystallographic results of Ref. [19] in which evidence was given that only the HGGGW portion

TABLE II
The set of simulated Cu-PrP complexes.

	System	N_{at}	N_{el}
S1	$Cu^{2+}(HG_1^-G_2^-G_3W)$(wat)	265	741
S2	$Cu^{2+}(HG_1^-G_2^-G_3W)$(wat) + 64 H_2O	467	1353
S3	$Cu^{2+}(HG_1^-G_2^-G_3)$	49	157
S4	$Cu^{2+}(HG_1G_2G_3)$ + 41 H_2O	172	485
S5	$[Cu^{2+}(HG_1^-G_2^-G_3)]_2$	98	314
S6	$[(HG_1^-G_2^-G_3)]_2$	96	296

Next to each system the number of atoms, N_{at}, and active electrons, N_{el}, are reported

of the octarepeat is directly involved in the Cu coordination in the N-terminal region. Similar conclusions have emerged from the works of Refs. [35, 37].

4.3.1. The Minimal Cu Binding Motif

To check the validity of the Cu coordination mode suggested by crystallography and unambiguously identify the amino acids directly bound to the metal, a number of model systems have been set up and studied with the help of ab initio simulations [33, 67]. The systems that have been simulated are listed in Table II. A minus sign on a glycine residue means that the backbone nitrogen of the corresponding amino acidic residue was deprotonated, while with (wat) the presence of an axially bonded water molecule in the starting configuration is indicated. To avoid any artificially high-reactivity of the terminal regions and mimic the presence of the rest of the peptide that was cut out, N- and C-terminus have been neutralized in the standard way, i.e., by adding CH_3—CO and CH_3—NH groups, respectively.

As we said, the initial configuration for the CP simulations of the S1, S3, and S4 model systems was the crystallographic structure of Ref. [19], whereas the CP dynamics of S2, S5, and S6 model systems was started from configurations taken from random-walk (RW) generated tetra-octarepeat structures (see ref [87, 88]. for details of the RW method). To analyze possible biases induced by the choice of the initial configuration, the CP dynamics of system S3 was also started from a RW configuration (see section 4.3.3 and Fig. 4).

We now briefly outline the kind of structural information that have been extracted from the simulations of the various systems listed in Table II.

4.3.2. $Cu^{2+}(HG^-G^-GW)$(wat) With and Without Solvent

The simulation of the system $Cu^{2+}(HG^-G^-GW)$(wat) without (S1) and with (S2) solvent was performed to test the stability of the crystallographic structure in which a water molecule is kept within the Cu coordination sphere by a Trp residue. Actually, there are indications that this geometrical structure, with the Trp indole ring lying parallel to the Cu binding plane, could be a spurious configuration

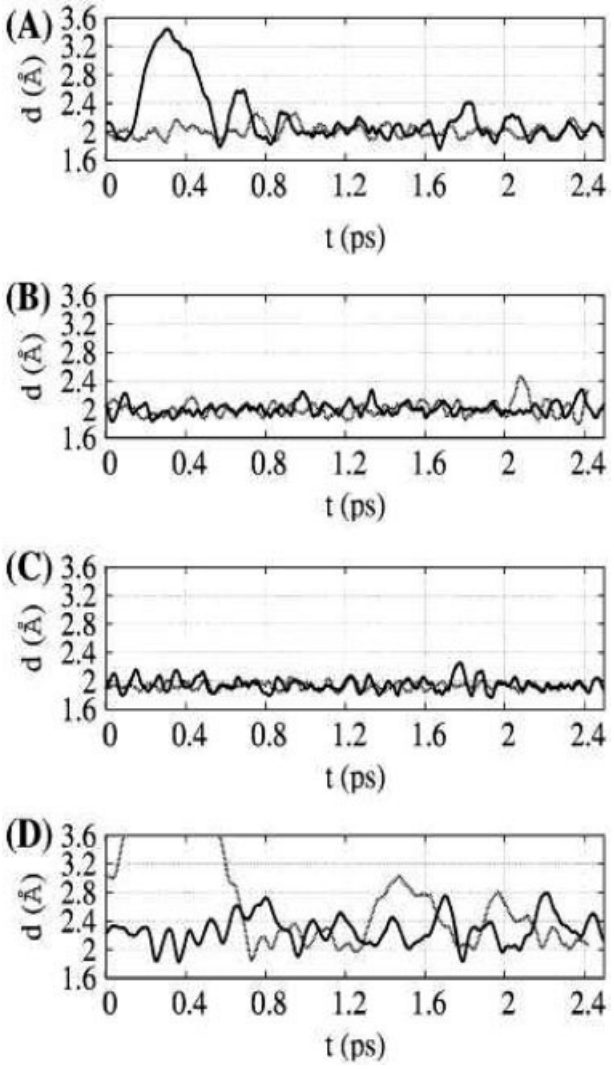

FIGURE 4. Time evolution at 300 K of distances between Cu and ligand atoms. The two reported trajectories started from the X-ray structure (solid line) and from one of the structures obtained through RW generation (dotted line). Distances Cu—N_δ(His) (A), Cu—$N(G_1^-)$ (B), Cu—$N(G_2^-)$ (C), and Cu—$O(G_2^-)$ (D) are shown.

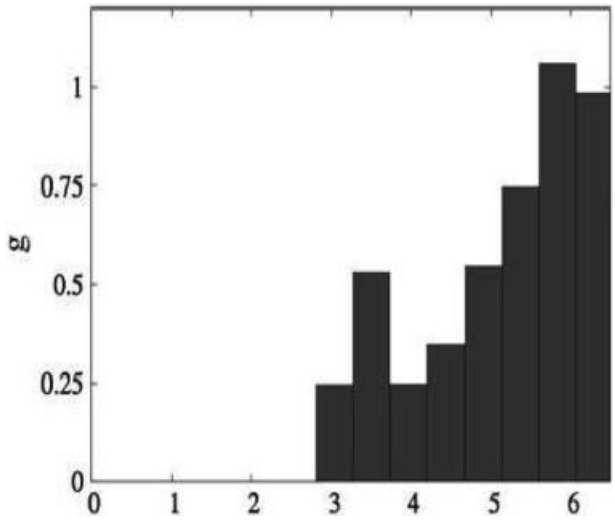

FIGURE 5. Radial distribution function, $g(r)$, of the distance, r, between Cu and water oxygens in the solvated S2 system.

related to the crystallization procedure [89, 90]. This conclusion is supported by the CP-MD simulations carried out in Ref. [33] on the S1 system, where the Trp "gate" is seen to open up letting the axial water to fly away. To verify whether this water molecule could possibly be replaced by an other water from the solvent, the simulation was repeated for a longer time at a temperature of 300 K and in the presence of 64 water molecules mimicking the solvent (S2). The $g(r)$ radial distribution of the distance between Cu and water oxygens shows that none of the 64 molecules replaces the water that had left the Cu coordination sphere (Fig. 5).

The conclusion of these two first sets of simulations is that the presence of a water molecule within the Cu coordination sphere and, consequently, of a nearby Trp indole group is a spurious feature of crystallization. Thus, all the successive simulations have been performed on the reduced tetra-peptide HGGG.

4.3.3. $Cu^{2+}(HG^{-}G^{-}G)$

It is important to test the dependence of CP-MD results on the initial atomic arrangement, by comparing trajectories generated starting from different initial structures. For this purpose, a detailed comparison was made between two CP-MD simulations of the S3 system in vacuum, where one was started from the crystallographic structure and the second from a configuration chosen among the several ones generated according to the protocol described in Refs. [87, 88]. The behavior with time of the Cu—N_{δ}(His), Cu—N(G_1^-), Cu—N(G_2^-), and Cu—O(G_2^-) distances, which was continuously monitored along the two CP trajectories, is displayed in Figure 4.

Reassuringly, we see that the whole time history of all the monitored distances is well-independent of the initial configuration. We also observe that Cu-ligand distances are rather stable with, however, the oscillations of the distances from Cu of the two Gly nitrogens faster and of smaller amplitude than that of the His nitrogen. This is an indication that the Cu binding to the Gly nitrogens is stronger than the one to the nitrogen of the His imidazole ring. The visibly wider and slower oscillation of the carboxyl oxygen-Cu distance confirmed the already known relative weakness of this bond.

4.3.4. $Cu^{2+}(HGGG) + 41\ H_2O$

The Cu^{2+}(HGGG) system with protonated backbone nitrogens and in the presence of 41 explicit water molecules (S4) was studied, to test the hypothesis that the interaction with copper induces the exchange of Gly nitrogen protons with the surrounding water molecules (Fig. 6). By monitoring the distance of the hydrogen from the G_2 nitrogen, the exchange was seen to happen after about 0.9 ps

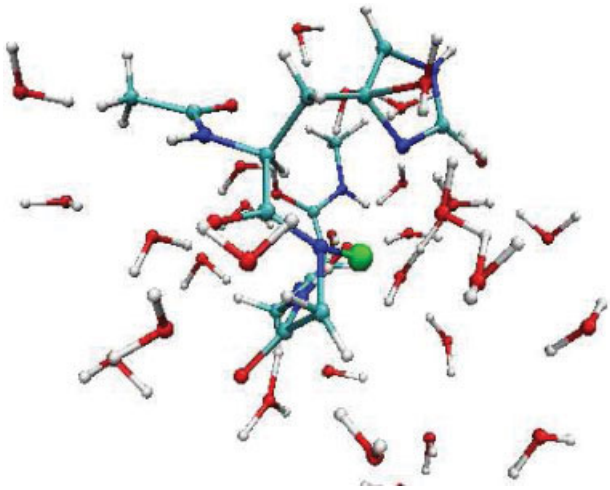

FIGURE 6. A Cu ion bonded to the HGGG tetra-peptide, solvated in explicit water. Colors are as follows, green is Cu, red is oxygen, blue is nitrogen, light blue is carbon, and white is hydrogen. [Color figure can be viewed in the online issue, which is available at www.interscience.wiley.com.]

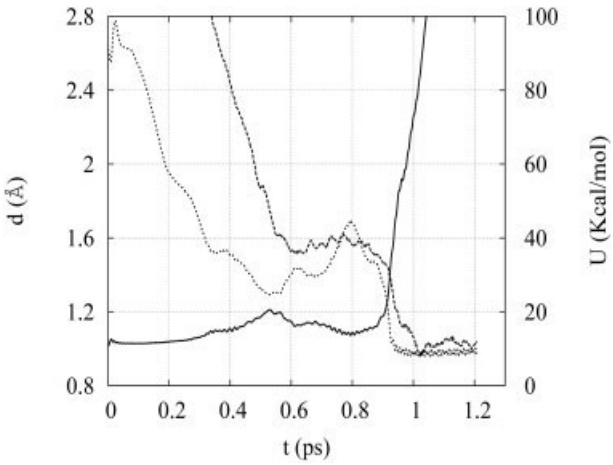

FIGURE 7. Time evolution of $H(G_2)$—$N(G_2)$ (solid line) and $H(G_2)$—O(wat) distances (dotted line) in the simulation of the Cu(HGGG) system at $T = 50$ K in water solvent. The *y*-axis on the right is in units of the total energy (dashed line) of the system.

of CP dynamics at 50 K. One finds that hydrogen enters the coordination sphere of a water molecule leaving the coordination sphere of the G_2 nitrogen (Fig. 6).

4.3.5. Dimeric System

Perhaps, the most interesting results that have been obtained in these studies concern the dynamics of the $[Cu^{2+}\ (HG^{-}G^{-}G)]_2$ system (which for simplicity was studied in vacuum). In fact, the available simulations show that, on the time scale of few ps, formation of a dimer is possible at Cu full occupancy concentration (one ion per HGGG peptide). Indeed, exchange of ligands between the two Cu ions (already visible after 0.86 ps at $T = 300$ K, see Fig. 8) is responsible for keeping the two tetrapeptides close to each other. Such a dynamical nature of the copper coordination is in agreement with what was observed in the simulations of the copper binding site in the His rich PrP region carried out in Ref. [91]. In the absence of Cu, instead, long-range electrostatic and dispersive interactions are unable to keep the two HGGG peptides close together, which then, within the same simulation time, separate out from one another. Also in the case of the dimer, a preference for an amidic nitrogen binding is visible, while the bond with the imidazole ring of the His is easily broken. These features can be read off from the time behavior of the distances of the various coordinated atoms from the two copper ions (data not shown). A problem with these CP-MD simulations is the rather small Cu—Cu average distance (from 2.1 to 3 Å) which is observed. Although in spin unrestricted simulations this distance becomes slightly larger (2.4 to 3.4 Å), it still remains pretty much smaller than what is experimentally observed (from 4.4 to 6.4 Å, see [28]). We can summarize the results of the many simulations described above as follows:

- The square planar (3N1O) coordination is maintained while the axial water flies away.
- The Cu—$N(G^{-})$ bond is stronger than the Cu—N′5f(His) bond.
- The Cu—$O(G_2^{-})$ bond is rather weak.
- Evidence of $N(G_2)$ deprotonation was seen.
- Monomers can be held together in a dimeric structure by the presence of copper.

In conclusion, despite the limitations due to the very-short time duration of the collected CP-MD trajectory, a quite consistent picture emerges from these investigations. They give support to the idea that Cu^{2+}-mediated interactions can induce N-terminal tail conformational transitions, which appear to be relevant both for the functionality of the Prion protein as well as for its propensity to expose hy-

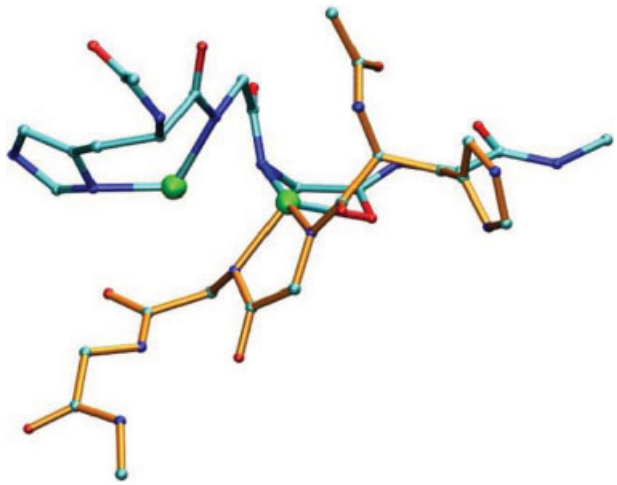

FIGURE 8. Sketch of the structure of the $[Cu^{2+}(HG^{-}G^{-}G)]_2$ system obtained in the spin-restricted simulation after 0.86 ps at $T = 300$ K. For clarity the two monomers have been differently colored. [Color figure can be viewed in the online issue, which is available at www.interscience.wiley.com.]

drophobic patches and consequently affect intermolecular interactions.

4.4. BINDING A SECOND HISTIDINE—GENERALITIES

As shown in section 3.3 (Fig. 3), however, experimental results clearly indicated that the relative concentration of Cu^{2+} and octarepeat (viz. the ratio $[Cu^{2+}]$:[octarepeat]) is an important parameter in determining the Cu binding geometry and eventually the metal rôle in the aggregation process.

In this second half of section 4, we describe the detailed analysis that was recently carried out to try to answer the question whether a second His can be stably bound to copper. Macroscopically, this corresponds to a situation where the [Cu]:[octarepeat] ratio is 1:2, at variance with the case analyzed in the previous section where this ratio was taken to be 1:1.

To have the simulated system of reasonable size, the second His was modeled as an isolated imidazole ring (Im), with a deprotonated N_δ pointing toward Cu and a CH_3 group attached to the C_γ atom. As we mentioned above, it is of special interest in this situation to study the dependence of the strength of this bond on the protonation state of nearby Gly nitrogen atoms. For this purpose, a stability study of the Cu-HisGGG-Im complex[2] with the first two Gly's in various protonation states was performed [34]. This analysis was done by comparing the results of systematic CP-MD simulations and geometric DFT optimization on the four systems of Table III.

As before with the symbol G^-, we mean that the hydrogen of the corresponding amide nitrogen has been removed. Thus, in SY1, both Cu-bound Gly's are deprotonated, whereas in SY4, they are fully protonated. In the case of SY2 and SY3, only one of the two Gly's involved in Cu-binding is deprotonated. The imidazole ring, introduced to mimic the presence of a second (possibly bound) His, is indicated by the symbol "Im." In the following, for short the Cu nearest-neighboring atoms are labeled according to the abbreviated notation introduced in Table IV.

TABLE III
The four model systems subjected to CP simulations.

System 1, SY1	Cu^{2+}(His $G_1^-G_2^-G_3$) + Im + 83 (H_2O)
System 2, SY2	Cu^{2+}(His $G_1G_2^-G_3$) + Im + 105 (H_2O)
System 3, SY3	Cu^{2+}(His $G_1^-G_2G_3$) + Im + 105 (H_2O)
System 4, SY4	Cu^{2+}(His $G_1G_2G_3$) + Im + 105 (H_2O)

TABLE IV
Atomic abbreviations.

Atom	Abbreviation
N_δ of the isolated imidazole ring	N(Im)
N_δ of the His	N(His)
N of the first Gly	N(G_1)
N of the second Gly	N(G_2)
Carbonyl O of the second Gly	O(G_2)
O from a water molecule	O(wat)
O from the N-terminal cap	O(Nterm)

We note that the SY2, SY3, and SY4 systems are (positively) charged, whereas SY1 is neutral, because the doubly charged Cu ion is neutralized by the negative charges of the two deprotonated Gly's. This makes an important difference from the technical point of view, especially when periodic boundary conditions are used, as it is most usually the case in numerical simulations. First of all, in fact, as already mentioned in section 4.2.2, it is necessary to have a larger separation between adjacent replicas when dealing with charged systems compared with the situation one encounters in the neutral case. Secondly, if energies of differently charged systems need to be compared, the Makov-Payne [92] correction has to be evaluated and taken into account.[3]

The minimal distance between nearest-neighbor replicas fixes the dimensions of the box surrounding the Cu complexes. The number of water molecules reported in Table III corresponds to the standard density of 1 g/cm^3.

4.4.1. Starting CP-MD Simulations

As we already stressed, given the foreseeable very short duration of CP-MD simulations (not

[2]From now on, we employ the three-letter code for the histidine residue, instead of the one-letter symbol (as we keep doing for short for Glycine) to avoid confusion with the symbol which is being used for hydrogen.

[3]Actually, the Makov-Payne correction applies also to systems with nonvanishing dipole moment, irrespective of their charge. For the systems of interest, here this bit of the correction is, however, very small.

TABLE V

Distances (in Å) of Cu from its nearest-neighbor atoms at the end of Phase (0) for the four systems of Table III.

	SY1	SY2	SY3	SY4
d[Cu-N(Im)]	2.16	2.22	2.13	2.05
d[Cu-N(His)]	2.25	2.22	2.14	2.17
d[Cu-N(G_1)]	2.51	2.66	2.54	2.79
d[Cu-N(G_2)]	1.96	1.82	1.99	2.00
d[Cu-O(G_2)]	3.25	3.22	3.40	3.29

more than a few ps at this moment), it is of the utmost importance to control the possible biases which are introduced as follows:

1. By the choice of the atomic configuration from which the CP dynamics is started.
2. By the procedure through which the system is brought at room temperature.

As for the first point, a good choice is to begin from either NMR or crystallographic PDB data, if available, or, lacking any such information, from some accurately equilibrated configuration so as to avoid as much as possible atomic stresses and instabilities. Consistently, with these general considerations, simulations were started from longly relaxed structures selected among the set of configurations generated according to the RW method described in Ref. [87] (and successfully employed in Ref. [33]).

According to the protocol outlined in section 4.2.1, it is useful to distinguish three main *Phases* in the simulation strategy that was followed.

Phase (0): preparation of the "initial" configuration; Phase (1): equilibration and thermalization steps; and Phase (2): CP-MD simulations at room temperature (300 K).

The "initial" configuration in Phase (0) used as input for the successive steps is the result of an atomic steepest-descent minimization carried out starting from the atomic coordinates of the selected RW configuration. The distances (in Å) of the Cu nearest-neighbor atoms, characterizing the "initial" geometry of the metal environment for the four systems SY1, SY2, SY3, and SY4 are given in Table V. The relevant atoms are labeled as indicated in Table IV.

TABLE VI

Summary of simulation history parameters.

	Phase (1)	Phase (2)
SY1	1.20 (100) + 0.60 (200)	1.50 (300)
SY2	0.60 (100) + 1.20 (200)	1.30 (300)
SY3	0.70 (100) + 0.70 (200)	1.45 (300)
SY4	0.70 (100) + 0.70 (200)	3.40 (300)

In Table VI, we summarize the information characterizing some key aspects of Phase (1) and Phase (2). We report for each system, in the second column what are the intermediate CP-MD simulation steps that have been followed to bring the system to room temperature (giving time durations and temperatures of preparatory simulations) and in the last column the duration of the final CP-MD trajectory at $T = 300$ K. Times are in picoseconds and simulation atomic temperatures are indicated in parenthesis.

4.4.2. Structural Optimization

To investigate the stability of a second His binding as function of the Gly's protonation state, the binding energy associated to the various Cu ligands must be computed. This is done by studying the energetics of the associated dissociation reactions. To make more transparent the set of virtual chemical reactions, we will be considering in the following, we introduce a synthetic nomenclature for the Gly protonation state in the peptide, as indicated in Table VII.

With the symbols introduced above, P indicates the doubly deprotonated Cu-peptide complex and H the nitrogen proton. With obvious notations, H on the left (on the right) of P represents the nitrogen

TABLE VII

Nomenclature of Gly protonation states.

P = Cu^{2+}(His $G_1^-G_2^-G_3$)	Both Gly's, G_1 and G_2, are deprotonated
HP = Cu^{2+}(His $G_1G_2^-G_3$)	The second Gly, G_2, is deprotonated
PH = Cu^{2+}(His $G_1^-G_2G_3$)	The first Gly, G_1, is deprotonated
HPH = Cu^{2+}(His $G_1G_2G_3$)	None of the Gly's are deprotonated

TABLE VIII

Dissociation reactions.

1.	HPH(Im)	→	HPH + Im	→	H + PH + Im	→	H + P + H + Im
2.				→	HP + H + Im	→	H + P + H + Im
3.	PH(Im)	→	PH + Im	→	P + H + Im		
4.	HP(Im)	→	HP + Im	→	H + P + Im		
5.	P(Im)	→	P + Im				

The symbols P, HP, PH, and HPH are defined in Table VII.

proton of the first Gly, G_1 (second Gly, G_2). Using this nomenclature, the dissociation reactions we want to study are summarized in Table VIII

4.5. BINDING A SECOND HISTIDINE—RESULTS

In presenting the conclusions of the extensive numerical investigation carried out in Ref. 34, it is convenient to separately discuss the structural results coming from the CP-MD simulations of the four systems SY1, SY2, SY3, and SY4 (section 4.5.1) and the analysis of the energetics of the dissociation reactions of Table VIII (section 4.6).

4.5.1. CP-MD Results

Let us start by discussing the results of the room temperature CP-MD simulations of the four Cu-complexes of Table III. The main objective of this analysis is the identification of the Cu ligands, i.e., the atoms that stably remain within the metal coordination sphere along the trajectory. Conventionally, the Cu coordination region has been taken as a sphere of radius 2.5 Å centered at the metal position.

The CP-MD time history of the distances from Cu of the atoms that among those listed in Table IV lay nearer to the metal are displayed in Figure 9 for the four SY1, SY2, SY3, and SY4 systems.

The figures clearly show (see also Table IX) that systems SY1 and SY2 remain tetra-coordinated (with N(Im), N(His), $N(G_1)$, $N(G_2)$ and N(Im), N(His), $N(G_2)$, $O(G_2)$, respectively) during the whole simulation (including thermalization steps, i.e., from Phase (0) to Phase (1)). For what concerns systems SY3 and SY4, we notice that, despite the fact that both of them start from a very similar "almost" fourfold Cu coordination (the Cu—$N(G_1)$ bond is only slightly "larger" than the radius of the metal coordination sphere for the latter, see Table V), the final geometries of the two systems are significantly different. The system SY3 ends up in a distorted tetrahedral configuration similar to that of the SY2 system. It should be noticed, however, that the Cu—O(Nterm) distance oscillates with lower-frequency and larger amplitude than the other Cu-ligand distances, thus suggesting a looser bonding for O(Nterm) (Fig. 9). On the contrary, in the system SY4, as the CP-MD simulation proceeds, two out of the four initial ligands are definitely lost, with in particular the Cu—$N(G_1)$ distance completely out of scale in the bottom-left panel. The reason for this markedly different behavior is that the fully protonated SY4 system is less stable than the singly deprotonated SY3 one.

We interpret the similar dynamical behaviors exhibited by systems SY1 and SY2 as a strong indication for a fourfold coordination mode of Cu to the HGGG binding site, which can be either (4N) or (3N1O), according to Gly's protonation state. This conclusion follows looking at the time evolution of the distances of the Cu bonded atoms displayed in the first two panels of Figure 9, where it is clearly visible that the metal likes to live in a tetra-coordinated structure in both cases.[4] This result will receive further support from the structural stability study, we will present in section 4.6.

A synthetic and useful way to represent the situation, one finds for the four systems of Table III is to give mean values ($\langle d \rangle$) and standard deviation (σ_d) of

[4]The main structural difference between SY1 and SY2 is that in the SY2 system $O(G_2)$ replaces the $N(G_1)$ atom of system SY1 (recall that it is G_1 that is protonated in SY2) as a fourth ligand. One can understand the occurrence of this modified coordination mode and the dynamics of $N(G_1)$ as the combined result of hindrance effects and the fact that, being deprotonated, G_2 is available for Cu binding. In fact, although the steric constraints coming from the binding of the nearby located N(His) and $N(G_2)$ atoms tend to keep $N(G_1)$ in the vicinity of Cu, the latter nitrogen is not able to stably enter the Cu coordination sphere. When this happens (like at $t \sim 0.4$, 0.85, and 1.15 ps, see second panel of Fig. 9), either N(Im) or $O(G_2)$, or both, are pushed out toward the boundary of the Cu coordination sphere.

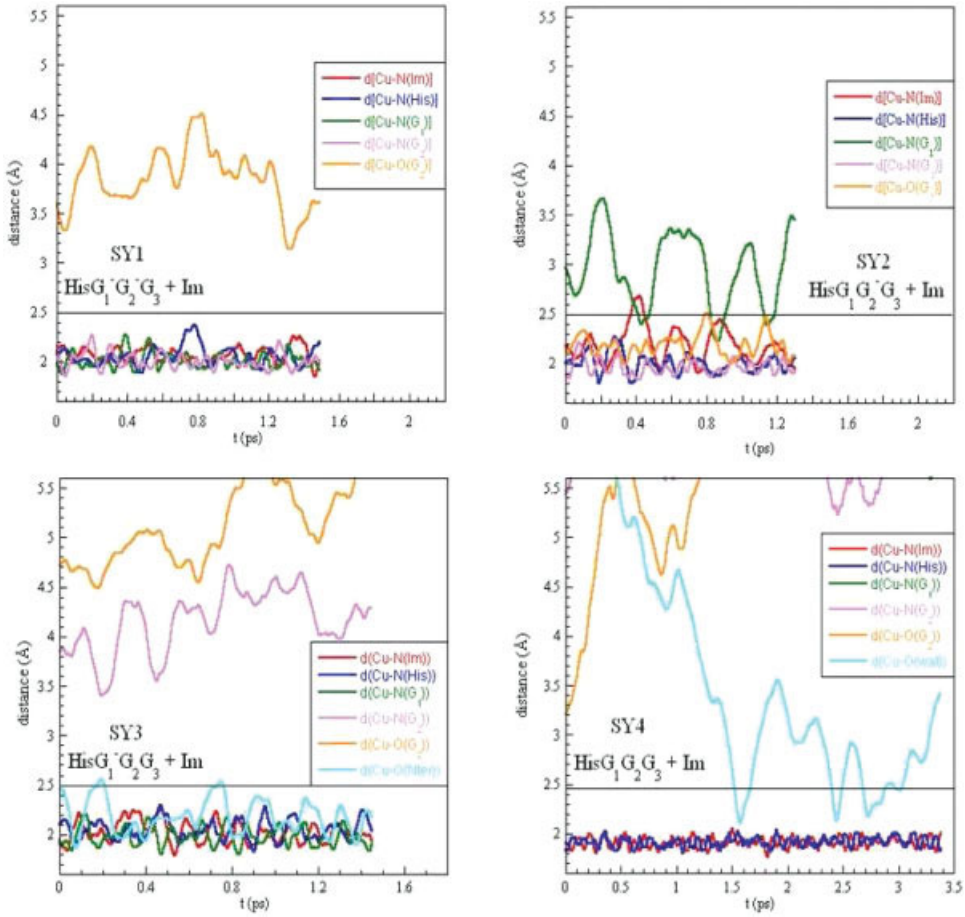

FIGURE 9. Time evolution of the distances from Cu of the selected atoms of Table V for the SY1, SY2, SY3, and SY4 systems along their respective room temperature CP-MD trajectories. [Color figure can be viewed in the online issue, which is available at www.interscience.wiley.com.]

the distances from Cu of the selected atoms of Table IV averaged along their room temperature CP-MD trajectories. The symbol "–" has been inserted in the entries corresponding to atoms that during the CP-MD do not stably live in the Cu coordination sphere. These data are summarized in Table IX.

TABLE IX

Mean values and standard deviation of the distances (in Å) from Cu of the selected atoms of Table VII averaged along the room temperature CP-MD trajectory for the SY1, SY2, SY3, and SY4 systems.

	SY1		SY2		SY3		SY4	
	$\langle d \rangle$	σ_d	$\langle d \rangle$	σ_d	$\langle d \rangle$	σ_d	$\langle d \rangle$	σ_d
d[Cu-N(Im)]	2.07	0.08	2.20	0.20	2.00	0.10	1.91	0.05
d[Cu-N(His)]	2.10	0.10	2.00	0.10	2.00	0.10	1.91	0.05
d[Cu-N(G_1)]	2.01	0.08	3.00	0.40	1.99	0.09	—	—
d[Cu-N(G_2)]	2.01	0.08	1.96	0.07	—	—	—	—
d[Cu-O(G_2)]	3.80	0.30	2.20	0.10	—	—	—	—
d[Cu-O(Nterm)]	—	—	—	—	2.20	0.20	—	—

4.6. BINDING A SECOND HISTIDINE—STRUCTURAL OPTIMIZATION AND STABILITY

By geometry optimization of representative configurations of the collected room temperature CP-MD trajectories, the contributions due to different ligands to the energy of the chemical species listed in Table VII, and hence the level of stability of the various Cu coordination modes encountered above can be investigated.

The configurational optimization is carried out in the standard way by minimizing the atomic DFT potential energy. The steepest-descent algorithm provided by the QE code was used for this purpose. At each atomic step, the electronic potential is recomputed using also here the steepest descent algorithm to solve the Kohn–Sham equations.

All the results can be summarized in two panels. In Figure 10, names, symbols, and energies of the optimized configurations are reported, whereas in Figure 11, the resulting Cu coordination modes and the distances between Cu and its ligands are given.

The flow-chart of Figure 10 displays the network of dissociation reactions whose energetics one needs to study. Boxes are labeled with the names of the various chemical species, according to the notation introduced in Table VII. Pairs of boxes connected by arrows represent dissociation reactions, with the successively dissociated products (i.e., the imidazole ring representing the second His and the protons of G_1 and G_2, indicated by Im and H, respectively) written next to the arrow.

Paths which can be followed from top to bottom along solid-line arrows are in a one-to-one correspondence with the five reactions of Table VIII. Boxes connected by broken-line arrows correspond to possible dissociation reactions in which, however, the energy of species in the lower box was not directly computed starting from the species in the upper box, but taken from already available CP-MD optimized configurations.

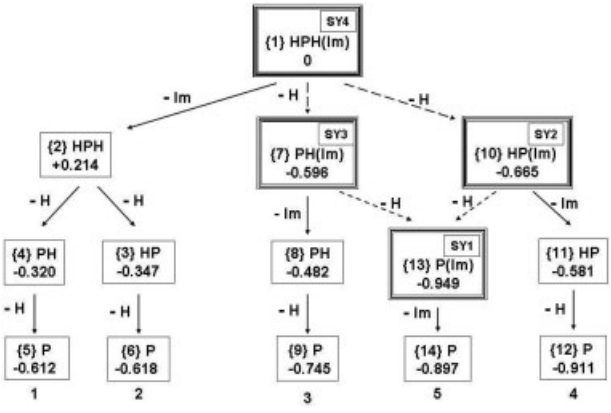

FIGURE 10. The flow-chart displaying the energetics of the network of dissociation reactions in study.

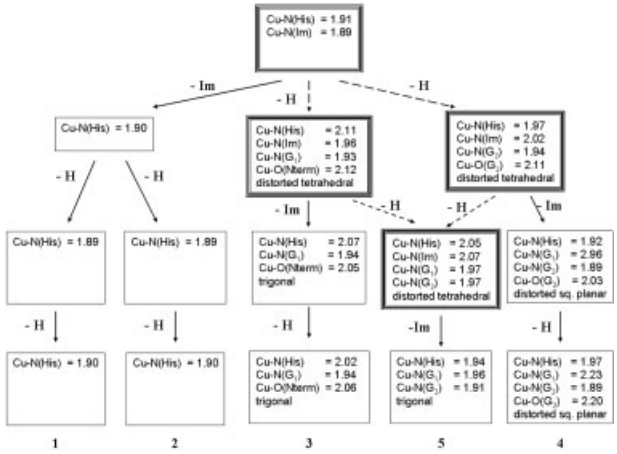

FIGURE 11. Cu coordination modes and Cu-ligand distances at the end of the optimization step.

The numbers (expressed in Rydberg[5]) written inside each box represent the difference between the (optimized) energy of the HPH(Im) species (in the following, {1} for short) at the top of the tree and the sum of the energy of the species in the box plus the energy of each of the extracted ligands along the branch. It should be noted that for each extracted H (we recall that by H here we mean a proton), we add the corresponding solvation energy because we are imagining that, as in real life, the proton is lost not in the vacuum, but in water.[6]

[5]1 Ry = 0.5 Hartree → 1312.73 kJ/mol.

[6]Solvation effects are neglected in energy calculations, even though the structures subjected to geometry optimization were taken from room temperature CP-MD simulations carried out in the presence of explicit solvent molecules. However, the solvation energy of H must be included, to account for the formation of the chemical bond between H and water. This bond has a dynamical nature and, therefore, the corresponding energy must be calculated consistently with the rest of the computation, i.e., by means of an appropriate CP-MD simulation. For this purpose, a system of 25 water molecules in a cubic box and at the density of 1 g/cm^3 was simulated for 2 ps at 300 K after an initial slow thermalization, as done in the SY1-SY4 simulations. The average total energy of the box, $\langle U(\text{wat})\rangle$, was computed. A proton was added to the initial system of 25 water molecules, the simulation was repeated and the total energy, $\langle U(\mathbf{H} + \text{wat})\rangle$, computed. The difference $U_s = \langle U(\mathbf{H} + \text{wat})\rangle - \langle U(\text{wat})\rangle$ is the energy contribution to the solvation free energy at 300 K for H. From the above procedure one gets $U_s = -1494$ kJ/mol.

The relative stability of species from top to bottom can be easily established by computing the difference $\Delta = E_{\text{bottom}} - E_{\text{top}}$, between the numbers appearing in the corresponding arrow-related boxes. If Δ is negative, the lower-level product is more stable than the higher-level reagent and vice versa.

4.6.1. The Geometry of Optimized Structures

In this section, we want to analyze and compare geometries and relative stability of the optimized structures of the Cu complexes appearing in the dissociation reactions of Table VIII from the energetic point of view. We will see that the conclusions one gets from this analysis are well in agreement with the results about the Cu coordination mode one extracts from the CP-MD room temperature simulations described in the previous sections.

For the reader's convenience, we summarize here below the key simulation results. The main conclusion of the whole CP dynamical study is that, if possible, Cu likes to be tetra-coordinated. Indeed,

1. we have seen that in the doubly deprotonated SY1 system the second imidazole displaces the loosely bound carbonyl oxygen turning the initial (3N1O) coordination into a (4N) tetra-coordination.
2. When G_1 is protonated, as it is the case for the system SY2, $N(G_1)$ gets replaced by $O(G_2)$ as a Cu ligand, leading to a (3N1O) coordination.
3. The situation appears to be different and more complicated in the case of the SY3 system, where only G_1, is deprotonated. The reason, however, is that, when the second glycine, G_2, is protonated, the ensuing breaking of the Cu—$N(G_2)$ bond induces also the breaking of the Cu-carbonyl oxygen bond originally present in the (3N1O) coordination.
4. When both G_1 and G_2 are protonated, a bicoordinated Cu binding site is visible because only N(His) and N(Im) are able to stably remain within the metal coordination sphere.

We now examine and comment the numbers collected in Figure 10. The main observation one can make is that in all cases the first step of the chain of reactions considered there, i.e., the dissociation of Im, leads to a product, which is less-stable than the initial reactant. In fact, the energy differences

$$\Delta E_n = E(\text{P}) - E(\text{P(Im)}) = 0.052 \text{ Ry} \quad (3)$$

$$\Delta E_n = E(\text{HP}) - E(\text{HP(Im)}) = 0.084 \text{ Ry} \quad (4)$$

$$\Delta E_n = E(\text{PH}) - E(\text{PH(Im)}) = 0.114 \text{ Ry} \quad (5)$$

$$\Delta E_n = E(\text{HPH}) - E(\text{HPH(Im)}) = 0.214 \text{ Ry} \quad (6)$$

are all positive as it can be seen from the data of Figure 10. Even if the imidazole binding energies are quite small, there is a clear indication that a second imidazole has the general tendency of stabilizing the Cu—PrP complex. It should also be noticed that the level of stabilization systematically increases going from the doubly deprotonated system (SY1) to the fully protonated one (SY4). In view of the CP-MD simulation results summarized above in this section, this is not an unexpected behavior. It simply means that the stabilization effect of the second imidazole is more effective when Cu finds himself in an "uneasy" coordination mode.

A number of further useful information fully consistent with the points 1 to 4 above can be drawn from the data collected in the panels of Figs. 10 and 11.

First of all, we notice that the dissociation of Im from the complex {13} (the structure of this compound is sketched in Fig. 12) along path 5, producing species {14}, significantly increases the energy of the system because the Cu—$O(G_2)$ bond cannot be formed anymore.

Secondly, although the energy stabilization of the Cu[HisGGG] complex by the Im addition amounts to only 68 kJ/mol when Im binds to P {14} (and 150 kJ/mol when it binds to PH {8}), the magnitude of the energy of the product {13} (i.e., of a complex involving two His sidechains around a single Cu^{2+} ion with four N ligand atoms in a (4N) coordination mode) is low-enough to justify its formation as an alternative to the (3N1O) coordination mode of Cu in NMR experiments and crystallography [19, 37] in situations, where only one His sidechain is available for binding.

Finally, the other interesting piece of information that can be extracted from the numbers in the flowchart of Figure 10 is that the putatively identical systems at the end of the five reaction pathways of Table VIII have energies that systematically decrease from left to right (notice, however, the ordering of the re-

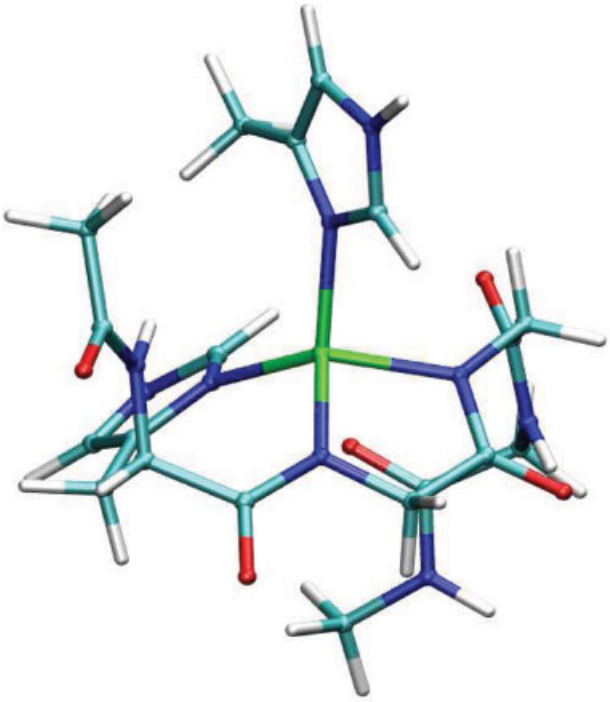

FIGURE 12. Optimized structure of compound P(Im) {13} displaying a distorted tetrahedral Cu^{2+} coordination. [Color figure can be viewed in the online issue, which is available at www.interscience.wiley.com.]

action pathways). Consistently, the Cu coordination number increases as indicated in Fig. 11).[7]

We wish to conclude this section with a general comment on the potentiality of the mixed approach pursued in Ref. [34] and illustrated in this review where ab initio calculations and DFT geometry optimizations are used in combination. The aim of this strategy is to overcome the major drawbacks of the two methods we are using, which are respectively the brevity of the CP-MD trajectory and the dependence of the DFT optimization step on the starting atomic configuration.[8]

The complementary use of ab initio calculations and DFT optimizations of structures selected according to a study of CP-MD trajectories, offers several advantages over the usual optimization procedure of manually built models. It should be noticed, in fact, that it is only through the dynamical history that one can follow along the CP-MD evolution, that the system configuration one wants to optimize can be appropriately chosen. An example in the analysis presented above is enough to make the point very clear. Let us consider the CP-MD history of the Cu ligands of system SY2 (Cu^{2+} (His $G_1G_2^-G_3$)+Im). Looking at the top-right panel of Figure 9, one can notice that the protonated G_1 nitrogen, $N(G_1)$, only enters from time to time the Cu coordination sphere, but it never becomes a stable ligand. It is then clear that the correct choice whereupon to start the optimization procedure is a configuration, where $N(G_1)$ is outside the coordination sphere. To validate the correctness of this choice in this peculiar case, we also tried an optimization step starting from the geometrical configuration reached by the SY2 system around 0.85 ps, that is where $N(G_1)$ is instead inside the Cu coordination sphere (namely at a distance of about 2.3 Å from Cu). At the end of the optimization, $N(G_1)$ is still within the Cu coordination sphere and Cu looks then penta-coordinated. The energy of this configuration is equal to that of the tetra-coordinated system {10}. So without the knowledge coming from CP-MD simulations, there would be no way to decide on the Cu coordination mode. This is a warning for a blind use of DFT optimization only. Further information about the dynamics of the system, if available, can be very useful.

4.6.2. The Bias-Induced by the Choice of the "Initial" Configuration

In this concluding section, we want to briefly address the problem of the possible bias induced by the choice of the "initial" configuration in ab initio simulations. As we have repeatedly said, given the very short length of any quantum-mechanical simulation, it is extremely important to check the stability of the results one gets upon changing the initial atomic configuration from which simulations are started. To investigate this issue, we have repeated the simulation of the system where G_1 is deprotonated (SY3) and that of the fully protonated system (SY4) starting from atomic steepest-descent relaxed configurations taken from the crystallographic structure of Ref. [19]. The coordinates of the atoms listed in Table IV at the end of Phases (0), slightly adjusted to accommodate the extra imida-

[7]The general question concerning the dependence of simulation/optimization results from the details of the initial system configuration and the ordering by which different numerical steps are successively carried out might be asked at this point. This important issue will be discussed in section 4.6.2.

[8]This last point is well-illustrated by the results summarized in Fig. 11. In fact, the compounds in the last row are all chemically identical (namely we are dealing with a fully deprotonated peptide with the second imidazole removed) but the final Cu coordination mode is different depending on the structure from which the optimization step was started.

TABLE X

Distances (in Å) from Cu of selected atoms for the system SY3′ and SY4′ at the end of Phases (0).

	SY3′			SY4′		
	Phase (0)	$\langle d \rangle$	σ_d	Phase (0)	$\langle d \rangle$	σ_d
d[Cu-N(Im)]	2.01	2.01	0.07	2.01	1.95	0.08
d[Cu-N(His)]	2.07	1.99	0.07	2.07	1.95	0.08
d[Cu-N(G_1)]	2.08	2.00	0.10	2.12	—	—
d[Cu-N(G_2)]	3.01	—	—	3.01	—	—
d[Cu-O(G_2)]	2.87	—	—	2.86	—	—

In the two successive columns for each system we give (for the atoms that do not end up outside the Cu coordination sphere) the mean value and the standard deviation of Cu-ligands distances averaged along the room temperature CP-MD trajectory.

zole ring present in the game, are reported in Table X. In the following for brevity, we will refer to these new model systems as SY3′ and SY4′.

The CP-MD time evolution at $T = 300$ K of the atomic distances listed in the first column of Table X is shown in Figure 13 for the system SY3′ (left panel) and SY4′ (right panel). We notice that, despite the fact that both systems start from a very similar "almost" fourfold Cu coordination (Table X), the final geometries of the two systems are significantly different. The SY3′ system ends up in a trigonal Cu coordination mode, whereas in the final configuration of the SY4′ system Cu is only doubly coordinated.

The reason for the difference between the history of systems SY3′ and SY4′ is, just like in the case of the SY3 and SY4 systems, that the fully protonated SY4′ system is definitely less stable than the corresponding singly deprotonated one.

If we now turn to a study of the energetics of the SY3′ and SY4′ systems as we did in the previous section for the SY3 and SY4 systems, one comes to the following conclusions (data not reported):

1. The coordination of the optimized SY3′ and SY4′ configurations is (2N) and (1N), respectively.
2. Consistently, the energy of the optimized configuration of the SY4′ system (−0.515 Ry) is slightly higher than that of the SY3′ system (−0.671 Ry).
3. The optimization step can hardly modify the metal coordination mode of the system.

The conclusion one can draw from the analysis presented in this section is that, although only energetic considerations are not enough to decide on the most stable geometry of the metal coordination mode, even not terribly long CP-MD trajectories can give reliable structural information, as they are rather stable against small modifications of the initial configurations if the latter are taken from experimentally known structures or longly thermalized classical MD simulations.

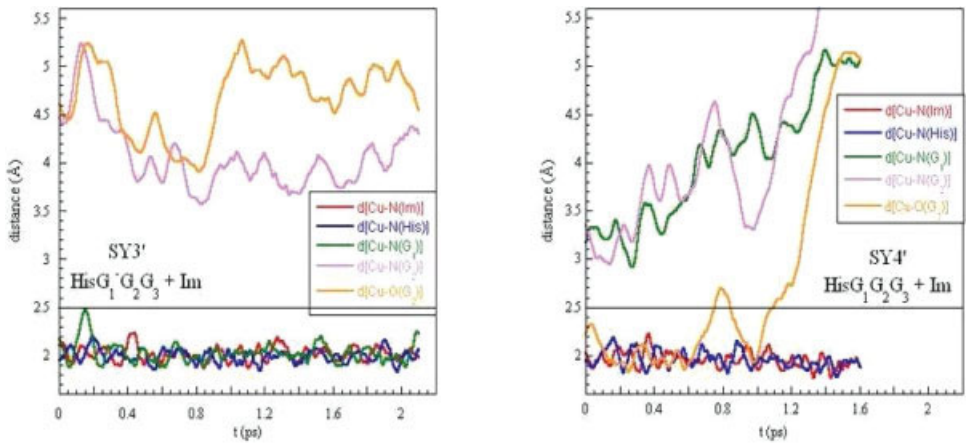

FIGURE 13. Time evolution of the distances from Cu of selected atoms for the SY3′ and SY4′ systems along their respective room temperature CP-MD trajectories. [Color figure can be viewed in the online issue, which is available at www.interscience.wiley.com.]

5. Conclusions and Outlook

Although we are still far from a clear understanding of the rôle of metals in protein misfolding and/or aggregation, the synergy between experimental and theoretical studies has reached a point where there seems to be hope that one can pinpoint the rather complicated structural scenario one encounters in the study of amyloid complexes. In particular, in the case of the Prion peptide combined experimental studies [27] and ab initio simulations [33, 34, 67] have convincingly proved that copper binding to the octarepeat region favors aggregation, possibly owing to an intermediate dimer formation mechanism [33], with the opposite being true when Cu binding occurs in the PrP core region [93].[9]

From a purely theoretical point of view, numerical simulations of Cu—PrP complexes have gone a long way, but it is still premature to try to draw any definite conclusion from the scanty set of available simulation data. Obviously, much longer and more accurate numerical investigations are necessary before one can have a satisfactory interpretation of the existing experimental information. However, we are at the moment in the very lucky situation in which, thanks to the spectacular development in computer design and the ongoing continuous progresses in the implementation of innovative algorithmic softwares, reliable ab initio studies of structural properties of macromolecules are really within our reach in a few years from now.

With a foreseeable forthcoming scaling up of the available CPU times by some 10^3 factor, one can hope to be soon able to simulate systems of biological interest of realistic size and for physical times of the order of the nanosecond.

The ultimate goal of the kind of complementary (experimental and theoretical) investigations, we have described in this review, is to go in the direction of providing new understanding on the fundamental biochemical processes which are at the basis of metal metabolism with the hope of finding new treatments for the devastating neurodegenerative diseases associated to protein aggregation and fibril formation.

[9]It may be interesting to note that in the case of the β-amyloid peptides, experimental information [40, 41] indicate a markedly different behavior depending on whether copper or zinc is involved in the game. While Cu is bound in a rather packed and stable configuration, Zn binding is more flexible and seems to be able to give rise to networks of cross-linked peptides [38].

ACKNOWLEDGMENTS

The authors like to thank all the many collaborators who have directly or indirectly contributed to the work reported in this review. Among them, special thanks are due to G. La Penna, G.C. Rossi, and F. Stellato. Use of *Cineca* cluster in Bologna, Fermi1 cluster at *E. Fermi Research Center* in Roma, BEN cluster at *ECT** in Trento, *CERM* cluster in Firenze, and SGI ALTIX 4700 at *LRZ* in Munich is gratefully acknowledged.

References

1. Prusiner, S. B. Science 1982, 216, 136.
2. Prusiner, S. B. Nobel Lectures, Physiology or Medicine 1996–2000; Ed Hans Jornvall; World Scientific Publishing Co.; Singapore, 2003.
3. Prusiner, S. B. Proc Natl Acad Sci USA 1998, 95, 13363.
4. Pan, K. M.; Baldwin, M.; Nguyen, J.; Gasset, M.; Serban, A.; Groth, D.; Mehlhorn, I.; Huang, Z.; Fletterick, R. J.; Cohen, F. E.; Prusiner, S. B. Proc Natl Acad Sci USA 1993, 90, 10962.
5. Gasset, M.; Baldwin, M. A.; Fletterick, R. J.; Prusiner, S. B. Proc Natl Acad Sci USA 1993, 90, 1.
6. Pepys, M. B. Philos Trans R Soc Lond B Biol Sci 2001, 356, 203.
7. Dominikus, A. L.; Schorn, C.; Nivon, L. G.; Esteve-Moya, V.; Christen, B.; Calzolai, L.; von Schroetter, C.; Fiorito, F.; Herrmann, T.; Güntert, P.; Wüthrich, K. Proc Natl Acad Sci USA 2005, 102, 640.
8. McKinley, M. P.; Meyer, R. K.; Kenaga, L.; Rahbar, F.; Cotter, R.; Serban, A.; Prusiner, S. B. J Virol 1991, 65, 1340.
9. (a) Chiesa, R.; Drisaldi, B.; Quaglio, E.; Migheli, A.; Piccardo, P.; Ghetti, B.; Harris, D. A. Proc Natl Acad Sci USA 2000, 97, 5574; (b) Chiesa, R.; Piccardo, P.; Quaglio, E.; Drisaldi, B.; Si-Hoe, S. L.; Takao, M.; Ghetti, B.; Harris, D. A. J Virol 2003, 77, 7611.
10. Nunziante, M.; Gilch, S.; Schatzl, H. M. J Biol Chem 2003, 278, 3726.
11. Eghiaian, F.; Grosclaude, J.; Lesceu, S.; Debey, P.; Doublet, B.; Tréguer, E.; Rezaei, H.; Knossow, M. Proc Natl Acad Sci USA 2004, 101, 10254.
12. Stockel, J.; Safar, J.; Wallace, A. C.; Cohen, F. E.; Prusiner, S. B. Biochemistry 1998, 37, 7185.
13. Miura, T.; Hori-i, A.; Mototani, H.; Takeuchi, H. Biochemistry 1999, 38, 11560.
14. Jackson, G. S.; Murray, I.; Hosszu, L. L.; Gibbs, N.; Waltho, J. P.; Clarke, A. R.; Collinge, J. Proc Natl Acad Sci USA 2001, 98, 8531.
15. Rachidi, W.; Mange, A.; Senator, A.; Guiraud, P.; Riondel, J.; Benboubetra, M.; Favier, A.; Lehmann, S. J Biol Chem 2003, 278, 14595.
16. Hornshaw, M. P.; McDermott, J. R.; Candy, J. M.; Lakey, J. H. Biochem Biophys Res Commun 1995, 214, 993.
17. Whittal, R. M.; Ball, H. L.; Cohen, F. E.; Burlingame, A. L.; Prusiner, S. B.; Baldwin, M. A. Protein Sci 2000, 9, 332.
18. Wells, M. A.; Jelinska, C.; Hosszu, L. L. P.; Craven, C. J.;

Clarke, A. R.; Collinge, J.; Waltho, J. P.; Jackson, G. S. Biochem J 2006, 400, 501.

19. Burns, C. S.; Aronoff-Spencer, E.; Dunham, C. M.; Lario, P.; Avdievich, N. I.; Antholine, W. E.; Olmstead, M. M.; Vrielink, A.; Gerfen, G. J.; Peisach, J.; Scott, W. G.; Millhauser, G. L. Biochemistry 2002, 41, 3991.
20. Qin, K.; Yang, Y.; Mastrangelo, P.; Westaway, D. J Biol Chem 2002, 277, 1981.
21. Viles, J. H.; Cohen, F. E.; Prusiner, S. B.; Goodin, D. B.; Wright, P. E.; Dyson, H. J. Proc Natl Acad Sci USA 1999, 96, 2042.
22. Kramer, M. L.; Kratzin, H. D.; Schmidt, B.; Romer, A.; Windl, O.; Liemann, S.; Hornemann, S.; Kretzschmar, H. J Biol Chem 2001, 276, 16711.
23. Garnett, A. P.; Viles, J. H. J Biol Chem 2003, 278, 6795.
24. Hasnain, S. S.; Murphy, L. M.; Strange, R. W.; Grossmann, J. G.; Clarke, A. R.; Jackson, G. S.; Collinge, J. J Mol Biol 2001, 311, 467.
25. Cereghetti, G. M.; Schweiger, A.; Glockshuber, R.; Van Doorslaer, S. Biophys J 2001, 81, 516.
26. Burns, C. S.; Aronoff-Spencer, E.; Legname, G.; Prusiner, S. B.; Antholine, W. E.; Gerfen, G. J.; Peisach, J.; Millhauser, G. L. Biochemistry 2003, 42, 6794.
27. Morante, S.; Gonzalez-Iglesias, R.; Potrich, C.; Meneghini, C.; Meyer-Klaucke, W.; Menestrina, G.; Gasset, M. J Biol Chem 2004, 279, 11753.
28. Chattopadhyay, M.; Walter, E. D.; Newell, D. J.; Jackson, P. J.; Aronoff-Spencer, E.; Peisach, J.; Gerfen, G. J.; Bennett, B.; Antholine, W. E.; Millhauser, G. L. J Am Chem Soc 2005, 127, 12647.
29. Lambert, M. P.; Barlow, A. K.; Chromy, B. A.; Edwards, C.; Freed, R.; Liosatos, M.; Morgan, T. E.; Rozovsky, I.; Trommer, B.; Viola, K. L.; Wals, P.; Zhang, C.; Finch, C. E.; Krafft, G. A.; Klein, W. L. Proc Natl Acad Sci USA 1998, 95, 6448.
30. Chromy, B. A.; Nowak, R. J.; Lambert, M. P.; Viola, K. L.; Chang, L.; Velasco, P. T.; Jones, B. W.; Fernandez, S. J.; Lacor, P. N.; Horowitz, P.; Finch, C. E.; Krafft, G. A.; Klein, W. L. Biochemistry 2003, 42, 12749.
31. Klein, W. L. In Protein Misfolding, Aggregation and Conformational Diseases—Part A; Uversky, V. N., Fink, A. L., Eds.; Springer-Verlag: Berlin, 2006; p 61.
32. Sigel, H.; Martin, R. B. Chem Rev 1982, 82, 385.
33. Furlan, S.; La Penna, G.; Guerrieri, F.; Morante, S.; Rossi, G. C. J Biol Inorg Chem 2007, 12, 571.
34. Furlan, S.; La Penna, G.; Guerrieri, F.; Minicozzi, V.; Morante, S.; Rossi, G. C. J Biol Inorg Chem 2009, 14, 361.
35. Aronoff-Spencer, E.; Burns, C. S.; Avdievich, N. I.; Gerfen, G. J.; Peisach, J.; Antholine, W. E.; Ball, H. L.; Cohen, F. E.; Prusiner, S. B.; Millhauser, G. L. Biochemistry 2000, 39, 13760.
36. Syme, C. D.; Nadal, R. C.; Rigby, S. E. J.; Viles, J. H. J Biol Chem 2004, 279, 18169.
37. Zahn, R. J Mol Biol 2003, 334, 477, and references therein.
38. Syme, C. D.; Viles, J. H. Biochim Biophys Acta 2006, 1764, 246.
39. Ma, Q. F.; Hu, J.; Wu, W. H.; Liu, H. D.; Du, J. D.; Fu, Y.; Wu, Y. W.; Lei, P.; Zhao, Y. F.; Li, Y. M. Biopolymers 2006, 83, 20.
40. Stellato, F.; Menestrina, G.; Dalla Serra, M.; Potrich, C.; Tomazzolli, R.; Meyer-Klaucke, W.; Morante, S. Eur Biophys J 2006, 35, 340.
41. Minicozzi, V.; Stellato, F.; Comai, M.; Dalla Serra, M.; Potrich, C.; Meyer-Klaucke, W.; Morante, S. J Biol Chem 2008, 283, 10784.
42. Morante, S.; Furenlid, L.; Schiavo, G.; Tonello, F.; Zwilling, R.; Montecucco, C. Eur J Biochem 1996, 235, 606.
43. Strange, R.; Morante, S.; Stefanini, S.; Hasnain, S.; Chiancone, E.; Desideri, A. Biochim Biophys Acta 1993, 1164, 331.
44. Bianconi, A.; Congiu-Castellano, A.; Dell'Ariccia, M.; Giovannelli, A.; Morante, S.; Burattini, E.; Durham, P. J. Proc Natl Acad Sci USA 1986, 83, 7736.
45. Meneghini, C.; Morante, S. Biophys J 1998, 75, 1953.
46. Giannozzi, P.; de Angelis, F.; Car, R. J Chem Phys 2004, 120, 5903.
47. Car, R.; Parrinello, M. Phys Rev Lett 1985, 55, 2471.
48. Del Pino, P.; Weiss, A.; Bertsch, U.; Renner, C.; Mentler, M.; Grantner, K.; Fiorino, F.; Meyer-Klaucke, W.; Moroder, L.; Kretzschmar, H. A.; Parak, F. G. Eur Biophys J 2007, 36, 239.
49. Boland, J. J.; Crane, S. E.; Baldeschwieler, J. D. J Chem Phys 1982, 77, 142.
50. Koningsberger, D. C.; Prins, R. X-ray Absorption. Principles, Applications, Techniques of EXAFS, SEXAFS and XANES; Wiley: New York, 1988, and references quoted therein.
51. Rehr, J. J.; Albers, R. C. Phys Rev 1990, B41, 8139.
52. Lee, P. A.; Pendry, J. B. Phys Rev 1975, 11, 2795.
53. Benfatto, M.; Natoli, C. R.; Bianconi, A.; Garcia, J.; Marcelli, A.; Fanfoni, M.; Davoli, I. Phys Rev 1986, B34, 5774.
54. Lee, P. A.; Citrin, P. H.; Eisenberg, P.; Kinkaid, B. M. Rev Mod Phys 1981, 53, 769.
55. Rehr, J. J.; Alberts, R. C. Rev Mod Phys 2000, 72, 621.
56. Benfatto, M.; Della Longa, S. J Synchrotron Radiat 2001, 8, 1087.
57. Benfatto, M.; Della Longa, S.; Qin, Y.; Li, Q.; Pan, G.; Wu, Z.; Morante, S. Biophys Chem 2004, 110, 191.
58. Gurman, S. J.; Binsted, N.; Ross, I. J Phys C 1986, C19, 1845.
59. Filipponi, A.; Di Cicco, A.; Natoli, C. R. Phys Rev 1995, B52, 15122.
60. Filipponi, A.; Di Cicco, A. Phys Rev 1995, B52, 15135.
61. Ankudinov, A. L.; Ravel, B.; Rehr, J. J.; Conradson, S. D. Phys Rev 1998, B58, 7565.
62. Binsted, N.; Strange, R. W.; Hasnain, S. S. Biochemistry 1992, 31, 12117.
63. Binsted, N. EXCURV98: CCLRC Daresbury Laboratory Computer Program; 1998.
64. (a) Durham, P.; Bianconi, A.; Congiu-Castellano, A.; Giovannelli, A.; Hasnain, S. S.; Incoccia, L.; Morante, S.; Pendry, J. P. EMBO J 1983, 9, 1441; (b) Strange, R.; Morante, S.; Stefanini, S.; Hasnain, S. S.; Chiancone, E.; Desideri, A. Biochim Biophys Acta 1993, 1164, 331.
65. (a) Martonak, R.; Laio, A.; Parrinello, M.; Kuo, I. F. W.; Mundy, C. J.; McGrath, M. J.; Siepmann, J. I.; VandeVondele, J.; Sprik, M.; Hutter, J.; Chen, B.; Klein, M. L.; Mohamed, F. R.; Krack, M.; Parrinello, M. J Phys Chem 2004, B108, 12990; (b) Aktah, D.; Passerone, D.; Parrinello, M. J Phys Chem 2004, A108, 848; (c) Kühne, T. D.; Krack, M.; Mohamed, F. R.; Parrinello, M. Phys Rev Lett 2007, 98, 066401.
66. (a) Carloni, P.; Blochl, P.; Parrinello, M. J Phys Chem 1995,

99, 1338; (b) Piana, S.; Bucher, D. P.; Carloni, P.; Rothlisberger, U. J Phys Chem 2004, B108, 11139; (c) Sharma, M.; Resta, R.; Car, R. Phys Rev Lett 2005, 95, 187401.

67. Furlan, S.; La Penna, G.; Guerrieri, F.; Morante, S.; Rossi, G. C. Eur Biophys J 2007, 36, 841.
68. (a) Ewald, P. P. Ann Phys 1921, 64, 253; (b) Allen, M. P.; Tildesley, D. J. Computer Simulation of Liquids; Clarendon Press: New York, 1988; (c) Darden, T.; York, D.; Pedersen, L. J Chem Phys 1993, 98, 10089; (d) Essmann, U.; Perera, L.; Berkowitz, M. L.; Darden, T.; Lee, H. L. G.; Pedersen, L. G. J Chem Phys 1995, 103, 8577.
69. (a) Gao, J. Comput Chem 1996, 7, 119; (b) Assfeld, X.; Rivail, J. L. Chem Phys Lett 1996, 263, 100; (c) Bash, P. A.; Ho, L. L.; MacKerell, A. D. J.; Levine, D.; Hallstrom, P. Proc Natl Acad Sci USA 1996, 93, 3698; (d) Field, M. J.; Bash, P. A.; Karplus, M. J Comput Chem 1990, 11, 700; (e) Freindorf, M.; Gao, J. J Comput Chem 1996, 17, 386; (f) Gao, J. Acc Chem Res 1996, 29, 298; (g) Gao, J.; Amara, P.; Alhambra, C.; Field, M. J. J Phys Chem 1998, A102, 4714; (h) Reuter, N.; Dejaegere, A.; Maigret, B.; Karplus, M. J Phys Chem 2000, A104, 1720.
70. Hohenberg, P.; Kohn, W. Phys Rev 1964, 136, 864.
71. Kohn, W.; Sham, L. J. Phys Rev 1965, 140, 1133.
72. (a) Parr, R. G.; Yang, W. Density Functional Theory of Atoms and Molecules; Oxford University Press: Oxford, 1989; (b) Dreizler, R. M.; Gross, E. K. U. Density Functional Theory; Springer-Verlag: Berlin, 1990; (c) Fiolhais, C.; Nogueira, F.; Marques, M. A. L. Primer in Density Functional Theory, Lecture Notes in Physics; Springer-Verlag: Berlin, 2003.
73. Runge, E.; Gross, E. K. U. Phys Rev Lett 1984, 52, 997.
74. Sportelli, L.; Neubacher, H.; Lohmann, W. Biophys Struct Mech 1977, 3, 317.
75. Pushie, M. J.; Rauk, A. J Biol Inorg Chem 2003, 8, 53.
76. Franzini, E.; De Gioia, L.; Fantucci, P.; Zampella, G. Inorg Chem Commun 2003, 6, 650.
77. Van der Spoel, D.; van Buuren, A. R.; Apol, E.; Meulenhoff, P. J.; Tieleman, D. P.; Sijbers, A. L. T. M.; Hess, B.; Feenstra, K. A.; Lindhal, E.; van Drunen, R.; Berensden, H. J. C. Gromacs User Manual, Version 3.1.1; Nijenborgh 4, 9747 AG Groningen: The Netherlands, 2002; Available at: http://www.gromacs.org.
78. Available at: http://ambermd.org/.
79. (a) Nosé, S. Mol Phys 1984, 52, 255; (b) Hoover, W. G. Phys Rev A 1985, 31, 1695.
80. Frenkel, D.; Smit, B. Understanding Molecular Simulation; Academic Press: San Diego, 1996.
81. Payne, M. C.; Teter, M. P.; Allan, D. C.; Arias, T. A.; Joannopoulos, J. D. Rev Mod Phys 1992, 64, 1045.
82. Mark, D.; Hutter, J. In Modern Methods and Algorithms of Quantum Chemistry; Grotendorst, J., Ed.; John von Neumann Institute for Computing: Jülich, Available at: http://www.fz-juelich.de/nic-series.
83. Baroni, S.; Dal Corso, A.; de Gironcoli, S.; Giannozzi, P.; Cavazzoni, C.; Ballabio, G.; Scandolo, S.; Chiarotti, G.; Focher, P.; Pasquarello, A.; Laasonen, K.; Trave, A.; Car, R.; Marzari, N.; Kokalj, A. Available at: http://www.pwscf.org/.
84. Available at: www.cpmd.org/.
85. Vanderbilt, D. Phys Rev 1990, B41, 7892.
86. Perdew, J. P.; Burke, K.; Ernzherof, M. Phys Rev Lett 1996, 77, 3865.
87. La Penna, G. J Chem Phys 2003, 119, 8162.
88. La Penna, G.; Morante, S.; Perico, A.; Rossi, G. C. J Chem Phys 2004, 121, 10725.
89. Riihimki, E.-S.; Martnez, J. M.; Klo, L. J Phys Chem B 2007, 111, 10529.
90. Marino, T.; Russo, N.; Toscano, M. Phys Chem B 2009, 111, 635.
91. Carloni, P.; Rothlisberger, U.; Parrinello, M. Acc Chem Res 2002, 35, 455.
92. Makov, G.; Payne, M. C. Phys Rev B 1995, 51, 4014.
93. Cox, D. L.; Pan, J.; Singh, R. R. P. Biophys J Lett 2006, 91, L11.